# Stimulation modulates adhesion and mechanics of hydrogel adhesives

Zhen Yang a‡, Xingwei Yang b‡, Rong Long b\*, Jianyu Li ac\*

<sup>a</sup>Department of Mechanical Engineering, McGill University, Montreal, QC H3A 0C3, Canada

<sup>c</sup>Department of Biomedical Engineering, McGill University, Montreal, QC H3A 0C3, Canada

## **ABSTRACT**

Ability to modulate the adhesion of soft materials on-demand is desired for broad applications ranging from tissue repair to soft robotics. Research effort has been focused on the chemistry and architecture of interfaces, leaving the mechanics of soft adhesives overlooked. Stimuli-responsive mechanisms of smart hydrogels could be leveraged for achieving stimuli-responsive adhesives that respond mechanically to external stimuli. Such stimuli-responsive adhesives involve complex chemomechanical coupling and interfacial fracture phenomena, calling for mechanistic understanding to enable rational design. Here we combine experimental, computational, and analytical approaches to study a thermo-responsive hydrogel adhesive. Experimentally we show that the adhesion and mechanical properties of a stimuli-responsive adhesive are both enhanced by the application of stimulus. Our analysis further reveals that the enhanced adhesion stems from the increased fracture energy of the bulk hydrogel and the insignificant residual stress on the adhesive-tissue interface. This study presents a framework for designing stimuli-responsive adhesives based on the modulation of bulk properties, and sheds light on the development of smart adhesives with tunable mechanics.

#### INTRODUCTION

Adhesive materials find significant use in engineering and medicine. They can be categorized into two classes: *mechanically passive adhesives* that are designed to maintain their structural and mechanical properties after placement, and *switchable adhesives* that allow for ondemand modulation of their bonding state and mechanical properties<sup>1</sup>. The former include pressure sensitive adhesives (PSAs)<sup>2</sup>, cyanoacrylate (super glue)<sup>3</sup>, and epoxy<sup>4</sup>, which are commonly used in daily life. The latter is exemplified with the Command Strip (3M Company) that can attach/detach under different loading conditions, as well as thermo-morphic PSAs that can reshape upon the temperature change<sup>5</sup>. Other switchable adhesives that can detach upon exposure of chemical, physical or mechanical stimuli<sup>6,7,8,9</sup> are under development. Recent efforts have been focused on interfacial mechanisms, such as chemical reactions and wrinkling, confined between the adhesive and the adherend. A knowledge gap exists for methodologies to enable on-demand

<sup>&</sup>lt;sup>b</sup>Department of Mechanical Engineering, University of Colorado Boulder, Boulder, CO 80309, USA.

<sup>&</sup>lt;sup>‡</sup>These authors contributed equally to this work

<sup>\*</sup> Corresponding authors

and predictive modulation of both the interfacial and bulk properties of the adhesive. This ability is desired for broad applications, ranging from tissue repair, regenerative medicine to soft robotics<sup>10,11</sup>.

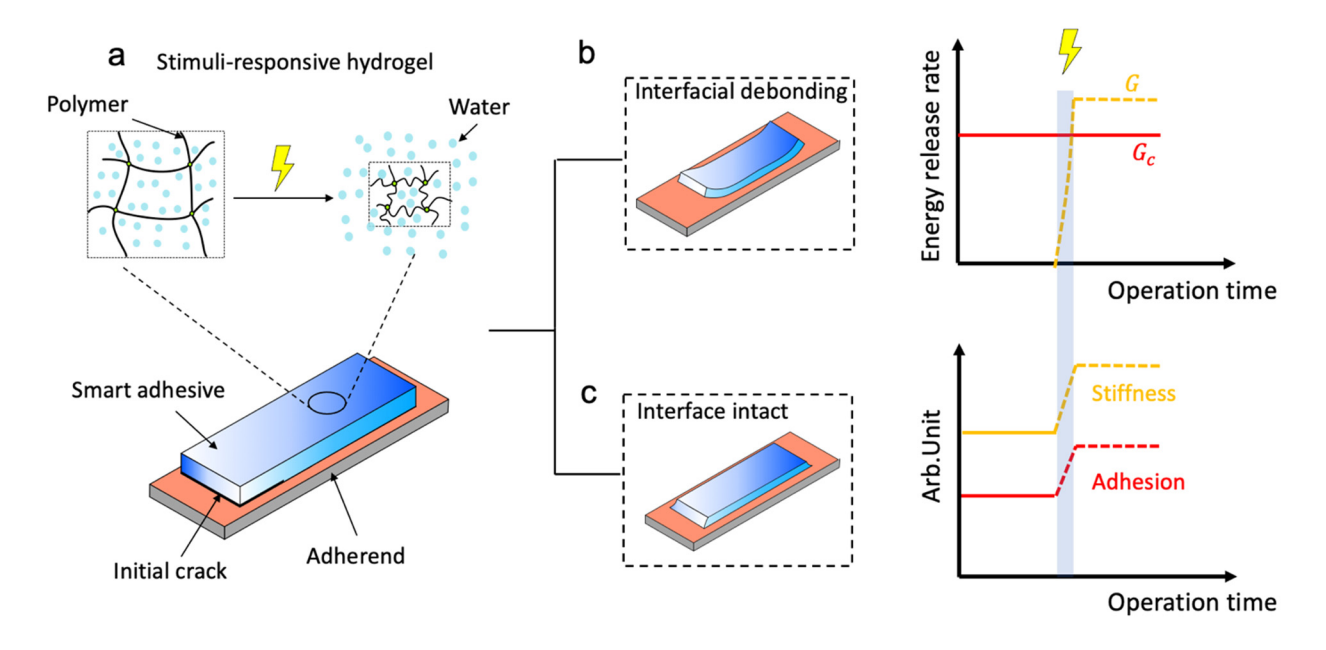


**Figure 1** Schematics of design and proposed responses of stimuli-responsive adhesives adaptive to external stimulation. (a) A stimuli-responsive adhesive is attached to an adherend, with an initial crack introduced at the interface and adhesion energy  $G_c$ . The adhesive matrix repels water and contracts upon stimulation. The stimuli-triggered contraction induces residual stress in the bulk hydrogel, yielding energy release rate G to drive the interfacial crack. (b) The interface debonds when G is greater than the interfacial adhesion energy  $G_c$ . (c) The interface stays intact when G is smaller than  $G_c$  and the adhesive hydrogel exhibits enhanced mechanical properties such as stiffness and adhesion energy.

Stimuli-responsive hydrogels are appealing for the development of switchable adhesives. They are also known as smart hydrogels, whose network can be regulated by chemical (ions, pH, proteins)<sup>12,13</sup> or physical (temperature, light, electrical or magnetic fields) cues<sup>14,15</sup>. The molecular-level regulation results in configurational transition of the hydrogel, as well as its mechanical properties. These hydrogels feature tunable mechanical properties<sup>6,16–19</sup>, dramatic volumetric change, and biocompatibility. They are well poised for drug delivery<sup>20,21</sup>, actuators<sup>22–25</sup> and soft robotics<sup>14,26</sup>. Recently, a thermo-responsive PNIPAm-based hydrogel was engineered into active wound dressings, which can adhere strongly to tissues and contract the edge of a wound in response to skin temperature, demonstrating accelerated wound closure *in vitro* and *in vivo*<sup>27</sup>. However, little is known about the effects of stimulation on the mechanical properties of the hydrogel adhesive. The interplay between the stimuli-responsive mechanism and the performance of the adhesive remains elusive and calls for further investigation.

Here we report a design of switchable adhesive, based on stimuli-responsive mechanisms of smart hydrogels. The stimulation applied externally could elicit phase transition and contraction of the adhesive matrix, thus modulating the bonding state and bulk properties of the adhesive. Specifically, together with the mechanical constraint by the adherend, the contraction could raise residual stress in the adhesive matrix, which yields an energy release rate G for an initial crack on the interface. We hypothesize that when G exceeds the adhesion energy  $G_c$ , the adhesive would debond, otherwise the mechanical properties of the adhesive such as stiffness and toughness could be modulated (Figure 1). To demonstrate the design principle of stimuli-responsive adhesives, we use a thermo-responsive adhesive consisting of PNIPAm-alginate double network hydrogel as a model system, hereafter referred to as the *dually crosslinked* (DC) hydrogel since both networks are crosslinked. This system can form strong tissue adhesion<sup>28,29</sup>, expel water and shrink at around 32  $^{\circ}$ C<sup>30</sup> due to PNIPAm.

To test our hypothesis, we combine experimental, theoretical, and computational approaches to study the stimuli-responsive behavior of the adhesive. We first characterize the mechanical properties of the stimuli-responsive adhesive before and after stimulation, demonstrating its responsiveness to temperature. We develop a finite element (FE) model to simulate the stimuli-responsive adhesive attached on a rigid substrate upon stimulation. By leveraging the FE model and an analytical model, we then evaluate quantitatively the effects of stimulation on the interfacial fracture process. We find a good agreement among experiments, FE simulations and analytical estimations. This work presents a comprehensive framework and valuable insights for designing stimuli-responsive adhesives and is expected to motivate the development of future adhesives with unprecedented properties.

## THEORETICAL SECTION

Free energy function. Following previous studies<sup>31–33</sup>, we assume the Helmholtz free energy of the hydrogel matrix of the stimuli-responsive adhesive to be the total free energy due to mixing of the polymer and the solvent  $(W_{mix})$  and stretching of the network  $(W_{stretch})$ :

$$W = W_{\text{mix}} + W_{\text{stretch}} \tag{1}$$

This assumption is also known as the Flory-Rehner model. The free energy due to stretching of the polymer chains is assumed to follow the Gaussian-chain model<sup>34</sup>:

$$W_{\text{stretch}} = \frac{1}{2} NkT \left[ \lambda_1^2 + \lambda_2^2 + \lambda_3^2 - 3 - 2\log(\lambda_1 \lambda_2 \lambda_3) \right], \tag{2}$$

Where N is the nominal chain density,  $\lambda_1$ ,  $\lambda_2$ ,  $\lambda_3$  are the principle stretches. The free energy due to mixing is formulated based on the Flory-Huggins model<sup>35,36</sup>:

$$W_{\text{mix}} = kT \left[ C \log \left( \frac{\Omega C}{1 + \Omega C} \right) + \frac{\chi C}{1 + \Omega C} \right], \tag{3}$$

where k is the Boltzmann constant, T is the absolute temperature,  $\Omega$  is the volume of a water molecule, C is the nominal number of water molecules per unit volume, and  $\chi$  is the Flory interaction parameter.

From Eqns. (1)-(3), the hydrogel matrix can be fully characterized once the Flory interaction parameter  $\chi$  and the nominal crosslink density N are specified. Since the PNIPAm network is thermo-responsive, the Flory parameter  $\chi$  is temperature-dependent, and is assumed to follow the form below<sup>37</sup>:

$$\chi(T,\phi) = \chi_0 + \chi_1 \phi \tag{4}$$

where  $\chi_0 = A_0 + B_0 T$ ,  $\chi_1 = A_1 + B_1 T$ , and  $\phi = 1/(1+\Omega C)$  is the volume fraction of the polymer in the hydrogel. Due to the presence of alginate, the four coefficients  $(A_0, B_0, A_1, B_1)$  for the PNIPAm-alginate hydrogel are expected to differ from those measured with the PNIPAm hydrogel, which are to be determined in the following experiment.

**Determination of Flory interaction parameter.** In the Flory-Rehner theory, the nominal chain density N is related to the shear modulus  $\mu$  by:

$$\mu = \frac{NkT}{I^{1/3}} = NkT\phi^{1/3}, \tag{5}$$

where  $J = \phi^{-1}$  is the equilibrium swelling ratio. The shear modulus can be measured using various methods such as rheological<sup>23</sup> or tensile<sup>38</sup> tests. The Flory interaction parameter  $\chi$  can be obtained by fitting the equations of states for ideal elastomeric gels<sup>39</sup>. The equation of states of the elastomeric gel is given by:

$$\sigma_{i} = \frac{\partial W_{\text{stretch}}(\lambda_{i}, \lambda_{j}, \lambda_{k})}{\lambda_{i} \lambda_{k} \partial \lambda_{i}} + \frac{dW_{\text{mix}}(J)}{dJ} - \frac{\varphi}{\Omega},$$
(6)

where  $\sigma_i$  is the true stress,  $\varphi$  is the chemical potential of ambient water, and i, j, k are the permutation notation 1, 2, 3. Note that repeated indices do not imply summation (i.e., the summation convention is not adopted here). By substituting Eqns.(2) and (3) into (6), we obtain the condition for the hydrogel to reach the swollen equilibrium at a specified temperature T, which together with the stress-free condition under free swelling yields a fitting function:

$$\frac{NkT}{J}(\lambda_f^2 - 1) + \frac{kT}{\Omega} \left[ \log\left(1 - \frac{1}{J}\right) + \frac{1}{J} + \frac{\chi_0 - \chi_1}{J^2} + 2\frac{\chi_1}{J^3} \right] - \frac{\varphi}{\Omega} = 0,$$
 (7)

where  $\lambda_f = J^{-1/3}$ . This equation can be characterized as follows. A hydrogel is submerged in an aqueous solution and swells to equilibrium at a certain temperature. The equilibrium swelling ratio J and the corresponding temperature T are recorded. Repeating the procedure for the same type of hydrogel under different temperatures enables the establishment of Eqn.(7), from which the Flory interaction parameter  $\chi$  can be fitted.

It needs to be pointed out that the direct characterization of  $\chi$  for the PNIPAm-alginate DC hydrogel is complicated by the fact that the ionic crosslinker of the alginate network, Ca<sup>2+</sup>, can migrate out from the DC hydrogel during swelling, thereby altering the crosslinking density of the hydrogel. To bypass the confounding effect, we adopted an alternative strategy by testing the

PNIPAm-alginate hydrogel without  $Ca^{2+}$  crosslinks, denoted as the *singly crosslinked* (SC) hydrogel. Furthermore, we submerged the SC hydrogels in an alginate solution of the same polymer content to equate the chemical potential of water in the hydrogel and in the solution, such that the chemical potential  $\varphi$  vanishes in Eqn.(7).

#### **EXPERIMENTAL SECTION**

Adhesion energy measurement. We adhered the adhesive onto the model tissue and divided the samples into two groups. The first group were kept at the room temperature before testing. The other group were stimulated at 37 °C for 3 hours and then returned to the room temperature, with the surface water removed by tissue paper. Before the adhesion measurement, a PET film was glued onto the back of the hydrogel to constrain the deformation. The model tissue was clamped onto a sliding tray and the hydrogel adhesive was peeled off using a universal testing machine (Model 5965; Instron, Norwood, MA, USA). During the peeling process, the angle between the adhesive and the tissue substrate was fixed at 90 degrees, and the loading rate was maintained at 0.5 mm·s<sup>-1</sup>. The force and the displacement were recorded.

Free swelling test. The SC hydrogel samples  $(10\times10\times10~\text{mm}^3~\text{in size})$  were submerged in 2% w/v alginate solution at different temperatures for one week such that the hydrogels had sufficient time to reach the equilibrium swelling. The samples were then taken out from the solution and blotted with tissue paper to remove the excessive liquid on the surface and were weighed immediately using an analytical scale at the room temperature to determine the mass  $m_{\rm gel}$ . After that, the samples were transferred to a freeze dryer (FreeZone 2.5L; Labconco, Kansas, MO, USA) for complete dehydration for 5 days, after which they were weighted again to determine the mass of the dry polymer  $m_{\rm dry}$ . The free swelling ratio was calculated using the gravimetric method:  $(m_{\rm gel}-m_{\rm dry})\rho_{\rm polymer}/m_{\rm dry}+1$ , where we have used  $\rho_{\rm water}=1~{\rm g/cm^3}$ ; the weighted average of the two polymers within the hydrogel  $\rho_{\rm polymer}=1.05~{\rm g/cm^3}$ .

Fracture energy measurement. The fracture energy of the DC hydrogel was measured using pure shear test<sup>40</sup>. Two samples were tested with one sample containing a notch and the other not. In the undeformed configuration, the hydrogel under the room temperature had a width of  $w=80~\mathrm{mm}$ , thickness of  $t=1.5~\mathrm{mm}$  and height of  $h=6~\mathrm{mm}$  (the distance between two clamps). In the notched sample, an initial crack of length 30mm was introduced by a razor blade, and the sample was pulled until rupture to record the critical stretch ratio  $\lambda_c$ . The unnotched sample was pulled to the same stretch ratio  $\lambda_c$ . The force and displacement were recorded. The fracture energy of the pure shear specimen can be calculated as:

$$\Gamma = W(\lambda_c)h, \qquad (8)$$

where  $W(\lambda_c)$  is the strain energy stored in the unnotched sample subjected to stretch  $\lambda_c$ , and can be evaluated by the area underneath the nominal stress-stretch curve up to  $\lambda_c$ .

**Rheological measurements**. The complex shear modulus of the SC hydrogel was measured using a rheometer (TA instruments). Cylindrical samples, 5 mm in diameter and 2 mm in thickness, were subjected to a constant shear strain of 1% with angular frequency ramping from 0.5 to 0.05 rad/s.

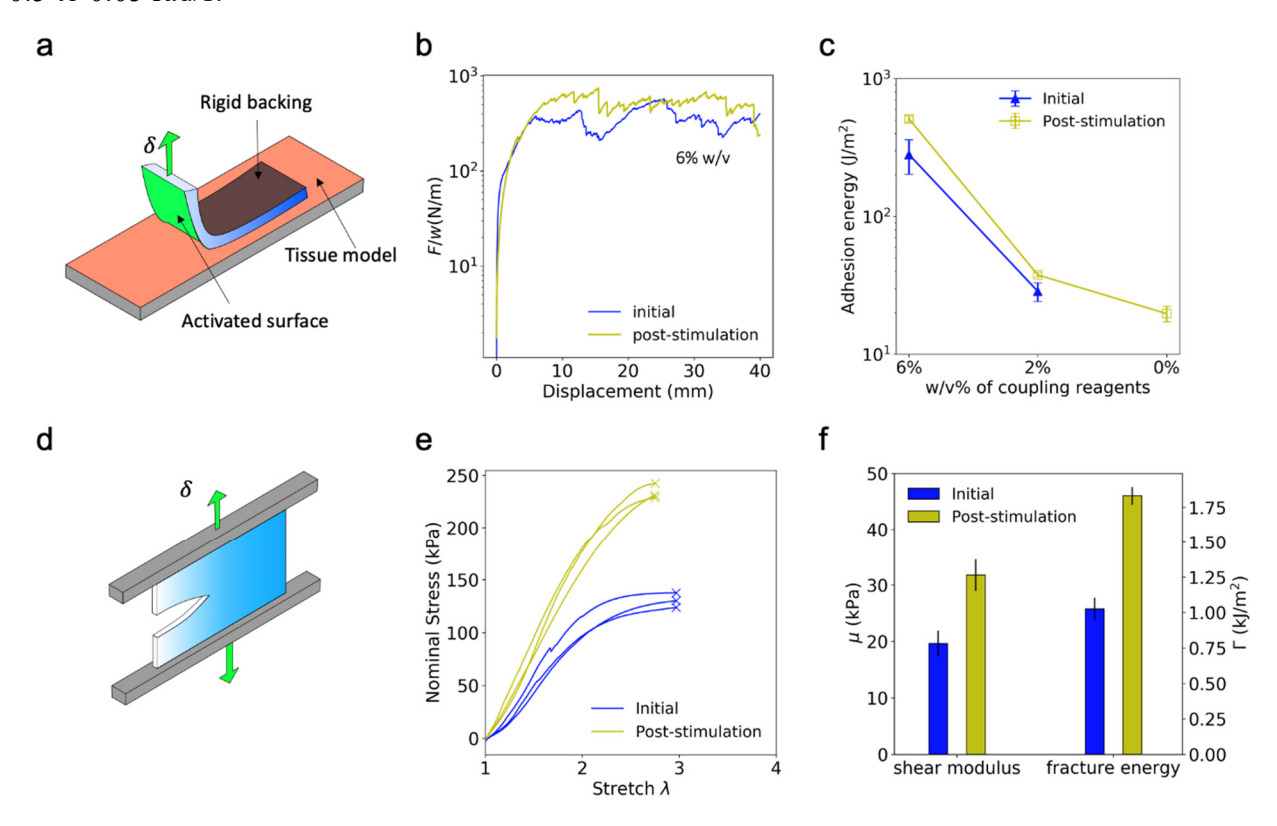


**Figure 2 Adhesion and fracture energy measurements** (a)-(c) The adhesion energy measurement. (a) Schematic of the 90-degree peeling test. (b) Representative curves of force/width versus displacement with topohesives containing 6% w/v reagents. (c) Initial and post-stimulation (PS) adhesion energies with topohesives containing different concentrations of the coupling reagents. (d)-(f) Fracture energy measurement. (d) Schematic of the pure shear test with a notched specimen. (e) Representative nominal stress-displacement curves for the unnotched specimens. The critical stretch corresponding to the onset of the crack propagation in the notched sample is marked using "x" marker. (f) Initial and post-stimulation (PS) shear modulus μ and fracture energy Γ for the PNIPAm/alginate DC hydrogel. Sample size N=3.

## RESULTS AND DISCUSSIONS

**Modulating adhesion via stimulation.** The adhesion between the hydrogel adhesive and the tissue surface is established by means of topological adhesion<sup>19</sup>, which consists of two parts. The first part is due to the interfacial bridging network (chitosan) formed in-situ, with its one end in topological entanglement with the hydrogel network, and the other end anchored on the tissue

surface via covalent bonding and physical interpenetration<sup>29</sup>. To drive an interfacial crack, either the hydrogel network or the stitching network needs to break. Then, the force needed to break the bridging network is transmitted into the bulk hydrogel, leading to the breakage of sacrificial bonds (the ionically crosslinked alginate hydrogel) and consequently substantial bulk energy dissipation<sup>29,41</sup>. The effects of stimulation are expected to be two-fold: the stimuli-triggered transition could alter the bulk properties of the adhesive, while resulting in a residual stress and an energy release rate to drive the interfacial crack, which offsets the adhesion energy of the stimuli-responsive adhesive. We first demonstrated the stimulation could trigger debonding of the stimuli-responsive adhesive. Given the absence of covalent bonding on the interface and a low adhesion energy  $G_c$ , the adhesive hydrogel came off the tissue substrate after phase transition at 37 °C, leaving behind an observable thin layer of water on the interface. The result supports our hypothesis shown in Figure 1(b) that the interface debonds when the stimulation-triggered G exceeds  $G_c$ .

We then hypothesized that the debonding could be arrested when  $G_c$  is sufficiently large, and that the post-stimulation (PS) adhesive is expected to exhibit higher stiffness and adhesion energy [Figure 1(c)]. To test the hypothesis, we characterized the adhesion property of the stimuliresponsive adhesives before and after stimulation when introducing covalent bonding to the interface (Supporting information). We observed that the stimuli-responsive adhesive applied on the tissue substrate experienced large volume changes (~50% volume reduction, see Figure S2). After returning to the room temperature, the volume reduction due to stimulation was retained, since the sample accessed no additional solvent. Notably, in the presence of a relatively weak interfacial adhesion (corresponding to 2% w/v coupling reagents in the topohesive), localized debonding was observed near the edge of the interface (Figure S3). When a strong interfacial adhesion is present (e.g., 6% w/v coupling reagents in the topohesive), such localized debonding was not observed.

We conducted the 90-degree peeling test to measure the initial and the PS adhesion energies [Figure 2(a)]. Figure 2(b) shows two representative force-displacement curves with the topohesive containing 6% w/v coupling reagents. The initial portion of the two curves fall together, but their plateaus values deviate from each other, with the peel force in the PS state being considerably higher. The adhesion energies with different concentrations of topohesives are calculated via<sup>42</sup>:

$$G_c = F_{p} / w, (9)$$

where  $F_P$  is the plateau peeling force and w the width of the adhesion region. Note that the width of the contact surface decreased slightly (~14.7 mm and 14 mm with 6% and 0% w/v reagents, respectively) compared to the initial value (~15 mm). Figure 2(c) shows that the PS adhesion energy is higher than the initial counterpart under all the tested conditions. For example, the averaged PS adhesion energies are 540 J/m² and 40 J/m² at 6 and 2% w/v of coupling reagents, respectively. They are higher than the initial values, 280 J/m² and 28 J/m², with the same concentrations of coupling reagent. Note that the initial adhesion energy with 0% w/v reagents is too low to be measured by the peeling test, hence not shown in the figure. Additionally, the

toughening effect was observed with varying concentrations of couple regent. As expected, the initial and PS adhesion energies both rise with increasing coupling reagents in use, due to enhanced interfacial bonding<sup>43,44</sup>. These results demonstrate that the adhesion is retained and even becomes stronger after stimulation, despite the significant deformation and possible localized debonding near the edges of the interface (Figure S2 and S3). To the best of our knowledge, this is the first observation of hydrogel adhesion toughening by a stimuli-responsive mechanism. Furthermore, the adhesive is believed to restore its initial state under the room temperature with the presence of enough water supply, e.g., in a humid ambient. Thus, the enhanced adhesion in the PS state can be suppressed for reciprocating smart adhesion.

It should be noted that the PS adhesion energy measured above might differ from the exact value corresponding to the interface between the stimulated adhesive and the substrate. The difference is attributed to the residual stress created by stimulation, which results in an energy release rate G for the edge crack (Figure 1) that tends to decrease the peel force and thus the measured adhesion energy. From the molecular perspective, this can be understood as the contraction of the bulk hydrogel matrix induced by stimulation pulls the stitching network, thus generating pre strain in it. As a result of which, one needs to apply a smaller peel force to drive the edge crack. The enhanced adhesion in the PS state indicates that G did not exceed the interfacial adhesion energy, because otherwise debonding would have occurred after stimulation. Nevertheless, the energy release rate G due to residual stress acts to offset the PS adhesion energy and thus needs to be quantified. It will be studied with analytical and computational models to be shown later.

Modulating mechanical properties via stimulation. To delineate the effect of stimulation on the bulk properties of the stimuli-responsive adhesive, we next characterize the shear modulus and the fracture energy of the adhesive hydrogel before and after stimulation using the pure shear test [Figure 2(d)]. Figure 2(e) shows that the nominal stress-stretch curve for the unnotched PS specimen exhibits larger initial slope, higher strength, but slightly lower stretchability. The measured shear modulus and the fracture energy are plotted in Figure 2(f). The initial shear modulus of the hydrogel is  $\mu_{initial} = 19$  kPa and increases to  $\mu_{PS} = 30$  kPa after stimulation [Figure S4 (a) and (b)]. The stiffening effect is attributed to the increased polymer content of the shrunken hydrogel, as indicated by Eqn.(5). Note the scaling relationship ( $\mu \propto \phi^{1/3}$ ) is applicable to hydrogels which were prepared in their dry state and stressed upon swelling<sup>45,46</sup>. In our case, however, the hydrogels were formed in the solution, thereby stressed in the dry state. In addition, there are also cases where the shear modulus of the hydrogel does not scale with  $\phi$ upon the exponent 1/3 depending on the properties of the precursor solution and of the state of observation  $^{47,48}$ , but all showing the positive correlation between  $\mu$  and  $\phi$ . As well, we observed a considerable increase in the fracture energy in the PS state. This positive correlation between the fracture energy and the polymer content can be interpreted with Lake-Thomas theory<sup>49</sup>. The detailed comparison is not pursued here as the DC hydrogel features substantial amount of bulk dissipation that dominates the fracture energy, which is not considered in the Lake-Thomas theory.

Future work is still required to investigate how the enhanced fracture energy is correlated to the change of the molecular structure of the DC hydrogel by applying stimulation.

Along with the measured adhesion energy, all the measured quantities of the adhesive are raised by the stimulation. Interestingly, we found they followed a similar scaling relation with respect to the swelling ratio J [Figure S4(c)]. The observations coincide with a recent work in our group<sup>50</sup>. In particular, we showed that a tough hydrogel composed of alginate-Ca<sup>2+</sup> and polyacrylamide (PAAM) exhibits a universal negative scaling relation of shear modulus, adhesion energy and fracture energy as a function of swelling ratio. The phenomenon was attributed to the unique double-network structure, in which the bulk dissipation dominates both the adhesion and fracture energies. Taken together, our results demonstrate that the stimulation allows for ondemand modulation of the mechanical properties of the stimuli-responsive adhesive, while leaving the interface bonding intact. To predict and control the behavior of the adhesive quantitatively, we next perform experiments to characterize the thermodynamic properties of the adhesive matrix in pursuit of finite element modelling.

Characterization of stimuli-responsive behavior. The free energy function of the adhesive matrix was characterized with rheological and free swelling tests. We focus on the SC hydrogel, which was composed of covalently crosslinked PNIPAm network but un-crosslinked alginate chains of the same polymer content as filler [Figure 3(a)]. The SC hydrogel swells freely in the alginate solution till equilibrium [Figure 3(b)]. Based on the postulation in the Flory-Huggins theory that the free energy due to mixing is independent of the crosslink density, it is reasonable to assume that  $\chi$  for the SC hydrogel resembles that of dually crosslinked (DC) hydrogel. As such, we can avoid the complication of ion exchange of the DC hydrogel during the swelling. Figure 3(c) illustrates the storage and the loss shear modulus  $\mu'$  and  $\mu''$  of the SC hydrogel measured using the rheometer. The storage modulus  $\mu'$  decreases monotonically with the frequency, and the low-frequency storage modulus linked with the crosslink density was estimated by linearly extrapolating the last three data points in the range of 0.05 - 0.13 rad/s. Besides, since  $\mu'$  is approximately 8 times larger than  $\mu''$  across the whole test frequency, we approximate the complex shear modulus with the storage modulus  $|\mu| = |\mu'| = 171$  Pa. Using Eqn.(5), the dimensionless crosslink density of the SC hydrogel is determined,  $N\Omega_{SN} = 3.9 \times 10^{-6}$ .

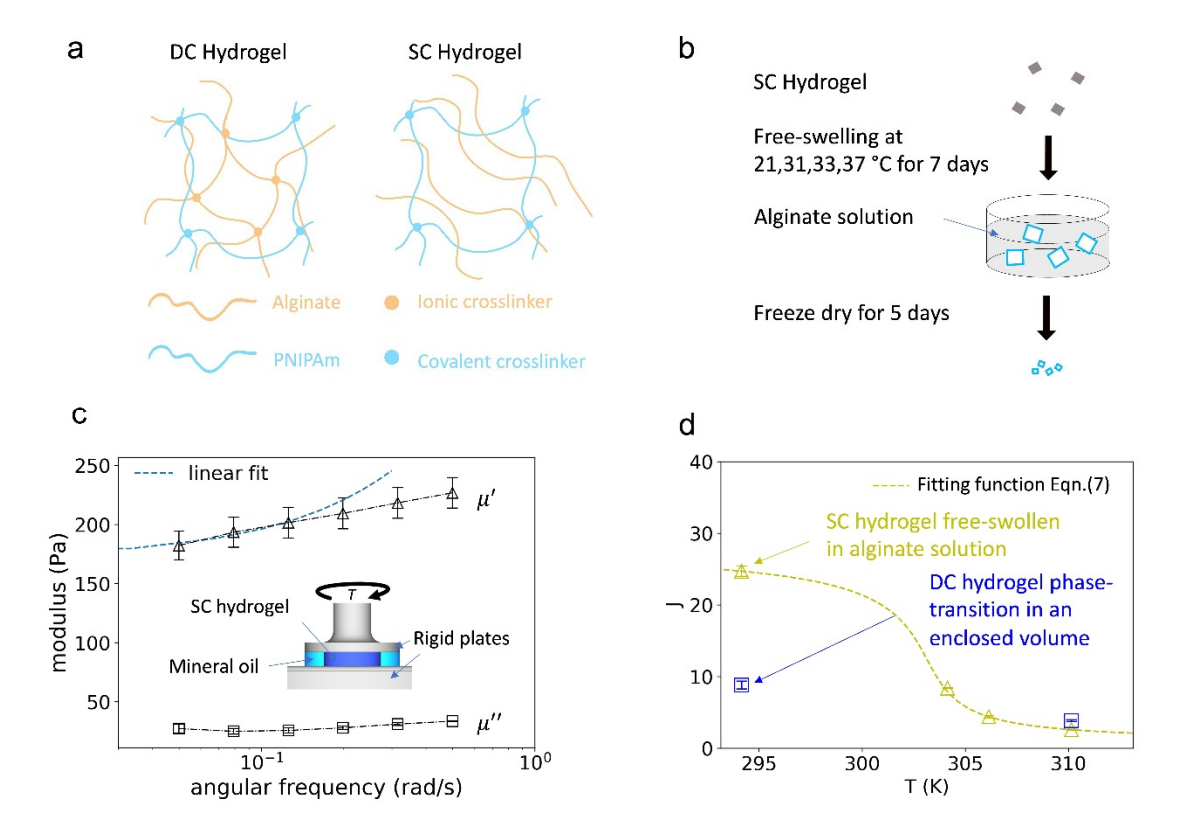


**Figure 3 Rheological and swelling measurements.** (a) Schematics of PNIPAm-alginate hydrogels with both covalent and ionic crosslinks (DC hydrogel), and with covalent crosslinks solely (SC hydrogel). (b) Schematic of the free swelling test using the SC hydrogel. (c) Complex modulus of the PNIPAm-alginate SC hydrogel measured using rheometer. (d) Equilibrium swelling ratio J for the SC hydrogel at different temperatures (yellow). The swelling ratio of the as-prepared DC hydrogel is also plotted at 294 K and 310 K (blue).

To establish Eqn.(7), we measured the equilibrium swelling ratio *J* for the SC hydrogel using free swelling tests at different temperatures. Figure 3(d) shows that the *J* value for the swollen-equilibrium SC hydrogel is initially 25 under the room temperature, then drastically decreases with the increasing temperature and eventually approaches 2 in the high temperature range. This is clearly different from the pure PNIPAm hydrogel, which approaches swelling ratio of 1 at elevated temperatures. The difference is attributed to the presence of the hydrophilic alginate polymer in the hydrogel. As well, we measured the swelling ratio *J* for the as-prepared DC hydrogel in the initial and the PS states, which is also plotted for comparison. Note that the asprepared DC hydrogel adhesive is not in the swollen-equilibrium state. Different from the swelling test, the DC hydrogel in the PS state is obtained by phase transition in an enclosed bag to avoid dehydration. The *J* value in the initial state for the as-prepare DC hydrogel is 8.8, which is considerably smaller than the equilibrium *J* value for the SC hydrogel due to the higher crosslink density. The *J* value in the PS state is comparable with the equilibrium *J* value for the SC hydrogel.

Lastly, we plugged the measured dimensionless crosslink density  $N\Omega_{SN}$  into the fitting function [Eqn.(7)] to fit the equilibrium swelling ratio J for the SC hydrogel. As can be seen, the fitted curve agrees very well with the experimental results [Figure 3(d)]. The fitted  $\chi$  is defined with the following parameters:  $A_0 = -1.95$ ,  $B_0 = 0.00868 \mathrm{K}^{-1}$ ,  $A_1 = -2.64$ ,  $B_1 = 0.00929 \mathrm{K}^{-1}$ . These efforts lead to the establishment of a free energy function of the stimuli-responsive adhesive matrix, which will be utilized in the finite element simulation later.

Analytical estimation of the energy release rate G. The problem analyzed here is illustrated in Figure 4(a). The two materials are assumed to be isotropic and elastic. The upper part represents the hydrogel adhesive with shear modulus  $\mu$  and initial thickness  $h_1$ , while the lower one represents the model tissue with initial thickness  $h_2$ . The model tissue is much stiffer than the hydrogel adhesive, and is hence approximated to be rigid in this analysis. We assume  $h_1 = h_2$  based on the dimensions of the specimen in the experiment. The bi-material specimen is subjected to a combined loadings and moments  $P_i$  and  $M_i$  (i = 1, 2, 3) (Figure S11).

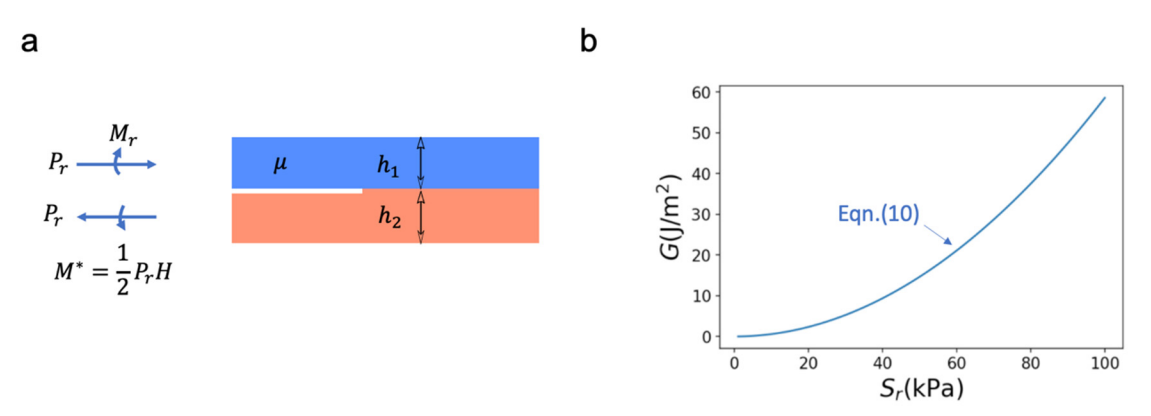


Figure 4 Analytical estimation of the strain energy release rate G on the hydrogel-tissue interface. (a) schematics of an interfacial crack embedded in a bi-material specimen subjected to the general and equivalent loadings. (b) the strain energy release rate G plotted against the residual stress in the hydrogel for  $h_1 = h_2 = 1.5$ mm.

Following Suo and Hutchinson<sup>51</sup>, the general loadings and moments applied to the bimaterial specimen are first converted to the equivalent loading and moment  $P_r$  and  $M_r$  [Figure 4(a)]. Upon stimulation, the hydrogel adhesive undergoes phase transition and shrinks. An analogy can be drawn from the shrunken adhesive to a residually stressed one, such that  $M_r = 0$  and  $P_r = S_r h_1$ , with  $S_r$  being the residual stress. By taking the difference between the energies stored far ahead of and far behind the crack tip, the strain energy release rate G is given by (Supporting information):

$$G = \frac{S_r^2 h_1}{8\mu} \,. \tag{10}$$

Eqn.(10) reveals that G is quadratic in  $S_r$  (Figure 4b) and the task to estimate G has become how to estimate the residual stress  $S_r$  in the hydrogel adhesive due to the shrinkage.  $S_r$  is estimated to

be 33 kPa for the adhesive hydrogel during the phase transition (Supporting information), thus the strain energy release rate G due to the residual stress in the PS state is  $G(S_r = 33 \text{ kPa}) = 6.6 \text{ J/m}^2$ . This value is much smaller than the measured adhesion energies with topohesives containing 6 and 2 % w/v coupling reagents [Figure 2(e)]. Importantly, it needs to be pointed out that Eqn.(10) is only valid for small deformation, so it only gives a first-order approximation (Figure S2). Provided that the hydrogel adhesive undergoes large deformation during the phase transition, for a more accurate estimation, the next section will show the implementation of the free energy function in the finite element model to estimate the strain energy release rate G.

Finite element simulation of the stimuli-responsive adhesive. We conduct finite element (FE) simulations with a commercial package ABAQUS (2020, Simulia). The Flory-Rhener free energy function [Eqn.(1)] is implemented in the FE model using a user-defined subroutine for hyperelastic materials (UHYPER). To validate the UHYPER subroutine, a free swelling test is performed for the DC and the SC hydrogels. Briefly, a cubic block of a hydrogel,  $8 \times 8 \times 8 \text{ mm}^3$  in size, is subjected to a temperature increase from 294 K to 320 K. The equilibrium swelling ratio J calculated from the FE model agrees well with those predicted by Eqn.(7) and measured in the experiments (Figure S6). The FE model simulates the swollen equilibrium state (*i.e.*, transient solvent migration process is not included in the simulations). We estimate the equilibrium swelling ratio of the initial DC hydrogel as  $J_0 = 10.1$ , by using the measured shear modulus  $\mu_{\text{gel}} = 19 \text{ kPa}$  and numerically iterating Eqns.(5) and (7). This value is not far from the experimentally measured swelling ratio  $J_0 = 8.8$  of the as-prepared DC hydrogel, which further justifies the use of the FE model.

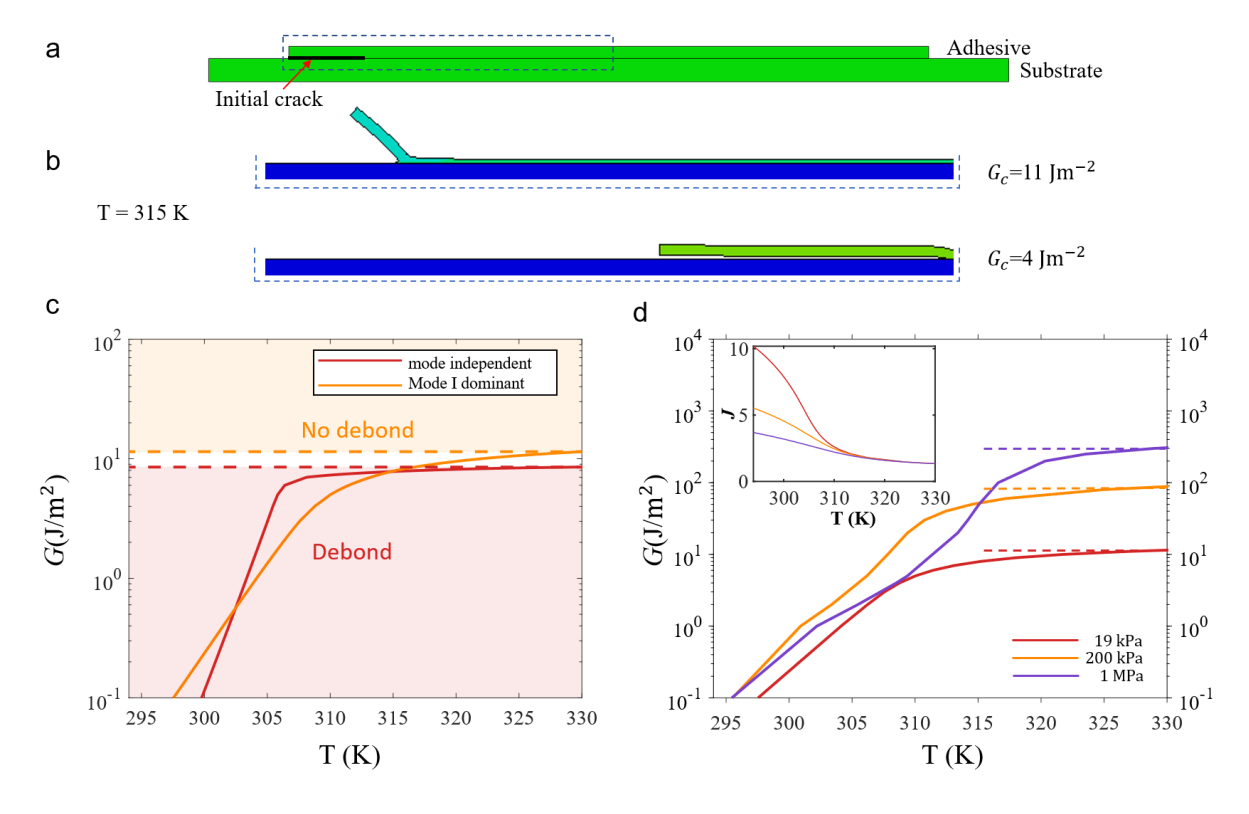


Figure 5 Finite element model of the stimuli-responsive adhesive. (a) FEM profile of the hydrogel adhesive and the substrate in the undeformed configuration. (b) Enlarged views of the crack tip region, boxed with dashed lines in (a), when temperature is at 315 K with  $G_c = 11 \text{ J/m}^2$  (top) and  $G_c = 4 \text{ J/m}^2$  (bottom) assuming a mode-independent crack. For  $G_c = 4 \text{ J/m}^2$ , most of the adhesive (99% in area) is detached from the substrate as temperature reaches to 315 K. (c) The strain energy release rate G on the adhesive-tissue interface for Mode-I dominant and mode-independent cracks with  $\mu = 19 \text{ kPa}$ . (d) The strain energy release rate G on the adhesive-tissue interface with different shear modulus given a Mode-I dominant crack. The adhesive matrix with higher moduli exhibits higher plateau values of G. The inset shows the equilibrium swelling ratio G of the DC hydrogels as a function of temperature.

With the validated model for the stimuli-responsive adhesive, we next build a twodimensional plane-strain model to simulate the adhesion between the adhesive and the model tissue. This model consists of an adhesive layer ( $80 \times 1.5 \text{ mm}^2$ ) on top and a rigid substrate ( $100 \times$ 3 mm<sup>2</sup>) underneath to represent the model tissue [Figure 5(a)]. At the interface, an edge crack of 10 mm is introduced in the left end, and the rest of the interface is bonded through a cohesive zone model, which is set as mode-independent and defined by a prescribed adhesion energy  $G_c$  (Figure S7). The cohesive zone model has been widely implemented to model bulk and interfacial cracks<sup>52–</sup> <sup>54</sup>. Notably, it was used to successfully model the peeling process of a tough hydrogel from a rigid substrate in recent studies<sup>41,55</sup>. A typical simulation starts from 294 K to higher temperature under a prescribed adhesion energy  $G_c$ . Figure 5(b) plots two simulations at 315 K but with different  $G_c$ values. The interfacial crack is trapped when  $G_c = 11 \text{ J/m}^2$  [Figure 5(b) top], but propagates when  $G_c = 4 \text{ J/m}^2$  [Figure 5(b) bottom]. As the temperature increases, the energy release rate G ramps from zero due to volume shrinkage of the adhesive matrix. When G reaches the prescribed adhesion energy  $G_c$  at a certain temperature, the interface crack starts to propagate. Therefore, the debonding is governed by the critical condition  $G = G_c$ . Note that the debonded portion of the adhesive undergoes free deswelling upon stimulation, which explains why the debonded adhesive for  $G_c = 4 \text{ J/m}^2$  [Figure 5(b) bottom] appears to be shorter than that for  $G_c = 11 \text{ J/m}^2$  [Figure 5(b) top].

Numerical estimation of the energy release rate G. After the establishment of the FE model, we leverage the critical debonding condition  $G = G_c$  to estimate the energy release rate G at a given temperature T. As can be seen below, the approach is facile to determine G without invoking sophisticated analysis. We conduct a series of above-mentioned FE simulations with varying adhesion energy  $G_c$ , which allows us to determine a specific temperature when the interfacial crack starts to propagate. Note that these simulations do not account for bulk hysteresis in the adhesive matrix (Figure S5), which have been shown to enhance the adhesion energy  $G_c$ . This is because our focus here is on estimating G at different temperatures and thus  $G_c$  is treated as a prescribed variable. The critical condition  $G = G_c$  for the onset of crack propagation is still valid in case of bulk hysteresis, as long as the contribution of bulk hysteresis is incorporated into  $G_c$ . Although the exact values of  $G_c$  under different testing conditions are not pursued here, it is worth noting

that they can be characterized by fatigue test and recently be incorporated into the FE simulations to determine the apparent adhesion energy<sup>57</sup>.

Given the severe modulus mismatch between the hydrogel and the model tissue, the interface crack is expected to be subjected to a mixed-mode fracture condition. To probe the effect of mixed-mode condition on the G estimation, we also conduct simulations with Mode-I dominant cohesive zone model, in addition to the mode-independent counterpart (Supporting Information). The Mode-I dominant model relaxes the resistance to slippage on the interface than the former, which could result in distinct deformation modes near the crack tip<sup>58</sup> (Figure S8 and S9). Figure 5(c) shows that the two types of cohesive zone models lead to a quantitative difference in the G estimation, which is attributed to the different deformation modes of the interface crack, as observed in Figures S8 and S9. However, the two cases, Mode-I dominant or mode-independent, follow a qualitatively similar trend, *i.e.*, G increases monotonically with the temperature T and then approaches a plateau at sufficiently high T in both cases. The plateau in G is due to the fact that the incremental volume shrinkage of the DC hydrogel becomes much smaller when T exceeds 310 K.

Rational design of the bonding of stimuli-responsive adhesive. These results provide a rational guideline to control the bonding state of the smart adhesive upon stimulation. When the adhesion energy is set beyond the plateau value, no debonding is found in simulation, indicating the phase transition is insufficient to drive the interfacial crack propagation. Specifically, the plateau value of G at high temperature is about 9 J/m² for the mode-independent crack, slightly lower than that of the Mode-I dominant crack ( $\sim$ 11 J/m²). These two plateau values, on the same order of magnitude as that estimated by the analytical model (6.6 J/m²), provide a threshold band of the adhesion energy  $G_c$  as illustrated in Figure 5(c). When  $G_c$  is below this band, crack propagation would occur under both the Mode-I dominant and mode-independent cases. When  $G_c$  is above this band, debonding would not occur in neither case.

Besides the adhesion energy  $G_c$ , the shear modulus of the adhesive matrix could be tuned to manipulate the bonding state. Since Eqns.(10) and Error! Reference source not found. imply that the energy release rate G induced by the residual stress is positively correlated to the shear modulus  $\mu$  of the DC hydrogel, we also vary  $\mu$  in the FE model and investigate the corresponding range of G. To this end, we set the shear modulus  $\mu$  to be 19 kPa, 200 kPa or 1 MPa (an accessible range for hydrogels) and plot the values of G at different temperatures in Figure 5(d). It should be noted that the equilibrium swelling ratio G is also affected by G as predicted by Eq. (7), i.e., the relative volume change due to phase transition decreases with increasing shear modulus [Inset in Figure 5(d)]. For example, if G = 19 kPa, the swelling ratio G changes from 10.2 to 2.5, as the temperature G increases from 294 K to 310 K. However, if G = 1 MPa, G changes from 3.7 to 2.2 over the same temperature range. Despite the smaller relative volume change accompanied with the increasing shear modulus, the plateau G value still increases considerably, i.e., from 10 J/m² for G = 19 kPa to 300 J/m² for G = 1 MPa. The result shows a good agreement with the trend predicted by Eqns.(10) and Error! Reference source not found. The study sheds light on

potential avenues to achieve high-level control over the adhesion and mechanics of adhesive materials.

Applicability of our results. Lastly, we discuss the applicability and implication of this work. The analytical and computational models above were built upon several assumptions. Firstly, the tissue is assumed to much stiffer than the adhesive. It is a reasonable assumption for skin and other tissues such as cartilage, which exhibit large moduli and/or potent strain-stiffening effects. Considering very soft tissues such as brain and adipose, the tissue substrate can deform to offset the deformation of the adhesive upon stimulation. Thus, a lower G is expected on the interface compared to the prediction from our analysis. While the toughening effect of the stimulation on the adhesive still holds, we expect robust adhesion of the stimuli-responsive adhesive, independent of stimulation, for other substrates with a wide range of stiffness. The point is supported by our prior work and other ongoing studies, showing robust adhesion of the stimuli-responsive adhesive on porcine skin and rodent skin in vivo<sup>27</sup>.

Secondly, we demonstrate the design principle of the stimuli-responsive adhesive using the PNIPAm-alginate hydrogel, because its stimulus, temperature, is easily controllable and its utility for wound management has been demonstrated. Given the diversity of stimuli-responsive hydrogels, our design is not limited to this specific material system, but can be applied to other material systems responsive to other stimuli such as pH and light, as long as they can form appreciable adhesion with different adhesive strategies<sup>27–29</sup>. Moreover, the analytical model developed in this work is applicable to other material systems, while the finite element model can be extended by incorporating the formulations for other stimuli-responsive mechanisms, as reported in the literature<sup>59</sup>.

## **CONCLUSIONS**

To summarize, we developed a design principle of switchable adhesives based on stimuliresponsive behavior of hydrogels. We demonstrated that the bonding of the adhesives can be modulated with stimulation, depending on the interfacial bonding. With sufficient initial adhesion energy, such adhesives were able to stiffen and toughen on-demand in response to external stimuli like temperature. In particular, the stimulation doubled the adhesion energy of the adhesive on a tissue-mimicking collagen substrate, suggesting the post-stimulation deswelling as a toughening mechanism. Also, we characterized the free-energy function of the stimuli-responsive adhesive, and developed both analytical and finite element models to quantitatively study the interplay between the stimulation and the interfacial fracture process. Our analysis determined the quantitative contribution of the stimulation to the strain energy release rate that drives the interfacial crack. We further presented strategies to modulate the interfacial fracture process, for instance, by tuning the modulus and thickness of the adhesive. The design principle of stimuliresponsive adhesives offers enormous design space to accommodate different stimuli-responsive hydrogels and adhesive strategies. Particularly, opportunities exist for non-covalent bond based hydrogel adhesives, as the relatively weak interfacial adhesion energy can withstand the low energy release rate due to stimulation, and the apparent adhesion energy can be enhanced due to the toughening mechanism induced by deswelling. This study establishes a rational design of stimuli-responsive adhesive and is anticipated to spark the interest and motivate the development of smart adhesives.

#### ASSOCIATED CONTENT

# **Supporting Information**

Materials, additional information on experiments, additional information on finite element modeling, additional information on analytical model.

## **AUTHOR INFORMATION**

# **Corresponding Author**

\*Email: <a href="mailto:rong.long@colorado.edu">rong.long@colorado.edu</a>. Tel.:303-492-3295 \*Email: <a href="mailto:jianyu.li@mcgill.ca">jianyu.li@mcgill.ca</a>. Tel.:514-398-1526

## **ORCID**

Zhen Yang: 0000-0003-4345-2130 Xingwei Yang: 0000-0002-9819-7993 Rong Long: 0000-0001-8992-2420 Jianyu Li: 0000-0002-1128-6804

## **Author Contributions**

<sup>‡</sup>These authors contributed equally to this work

## **Funding Sources**

This work was supported by Natural Sciences and Engineering Research Council of Canada (Grant RGPIN-2018-04146), Canada Foundation for Innovation (Grant 37719) and Fonds de Recherche du Québec – Nature et technologies (FRQ-NT NC-270740). Z. Y. acknowledged the support from McGill Engineering Doctoral Awards. J. L. acknowledged the support from the Canada Research Chair Program. X.Y. and R.L. were supported by a CAREER award (NSF CMMI-1752449) from the National Science Foundation of the United States.

#### **Notes**

The authors declare no competing financial interest.

## References

- (1) Croll, A. B.; Hosseini, N.; Bartlett, M. D. Switchable Adhesives for Multifunctional Interfaces. *Adv. Mater. Technol.* **2019**, 4 (8), 1–20.
- (2) Creton, C. P Ressure-Sensitive Adhesives : An Introductory Course. *MRS Bull.* **2003**, 434–439.

- (3) Ardis, A. E. Preparation of Monomeric Alkyl Alpha-Cyano-Acrylates, August 1, **1949**.
- (4) Tesoro, G. Epoxy Resins-Chemistry and Technology. *J. Polym. Sci. Polym. Lett. Ed.* **1988**, 26 (12), 539–539.
- (5) Joaquin Delgado, S. F. S. United States Patent (19) 11 Patent Number: BATTERY-49. United States Pat. **1994**, No. 19, 3–5.
- (6) Gao, Y.; Wu, K.; Suo, Z. Photodetachable Adhesion. Adv. Mater. 2019, 31 (6), 1–7.
- (7) Chen, X.; Yuk, H.; Wu, J.; Nabzdyk, C. S.; Zhao, X. Instant Tough Bioadhesive with Triggerable Benign Detachment. *Proc. Natl. Acad. Sci. U. S. A.* **2020**, 117 (27), 15497–15503.
- (8) Lin, P.-C.; Vajpayee, S.; Jagota, A.; Hui, C.-Y.; Yang, S. Mechanically Tunable Dry Adhesive from Wrinkled Elastomers. *Soft Matter* **2008**, 4, 1830.
- (9) Li, Q.; Zhang, P.; Yang, C.; Duan, H.; Hong, W. Switchable Adhesion between Hydrogels by Wrinkling. *Extrem. Mech. Lett.* **2021**, 43.
- (10) Donkerwolcke, M.; Burny, F.; Muster, D. Tissues and Bone Adhesives Historical Aspects. *Biomaterials* **1998**, 19 (16), 1461–1466.
- (11) Jones, V.; Grey, J. E.; Harding, K. G. ABC of Wound Healing: Wound Dressings. *Br. Med. J.* **2006**, 332 (7544), 777–780.
- (12) Shastri, A.; McGregor, L. M.; Liu, Y.; Harris, V.; Nan, H.; Mujica, M.; Vasquez, Y.; Bhattacharya, A.; Ma, Y.; Aizenberg, M.; Kuksenok, O.; Balazs, A. C.; Aizenberg, J.; He, X. An Aptamer-Functionalized Chemomechanically Modulated Biomolecule Catch-and-Release System. *Nat. Chem.* **2015**, 7 (5), 447–454.
- (13) Miyata, T.; Asami, N.; Uragani, T. A Reversibly Antigen-Responsive Hydrogen. *Nature* **1999**, 399 (6738), 766–768.
- (14) Han, D.; Farino, C.; Yang, C.; Scott, T.; Browe, D.; Choi, W.; Freeman, J. W.; Lee, H. Soft Robotic Manipulation and Locomotion with a 3D Printed Electroactive Hydrogel. *ACS Appl. Mater. Interfaces* **2018**, 10 (21), 17512–17518.
- (15) Dong, L.; Agarwal, A. K.; Beebe, D. J.; Jiang, H. Adaptive Liquid Microlenses Activated by Stimuli-Responsive Hydrogels. *Nature* **2006**, 442 (7102), 551–554.
- (16) Wada, S.; Kitamura, N.; Nonoyama, T.; Kiyama, R.; Kurokawa, T.; Gong, J. P.; Yasuda, K. Hydroxyapatite-Coated Double Network Hydrogel Directly Bondable to the Bone: Biological and Biomechanical Evaluations of the Bonding Property in an Osteochondral Defect. *Acta Biomater.* **2016**, 44, 125–134.
- (17) Lin, S.; Liu, J.; Liu, X.; Zhao, X. Muscle-like Fatigue-Resistant Hydrogels by Mechanical Training. *Proc. Natl. Acad. Sci. U. S. A.* **2019**, 116 (21), 10244–10249.
- (18) Matsuda, T.; Kawakami, R.; Namba, R.; Nakajima, T.; Gong, J. P. Mechanoresponsive Self-Growing Hydrogels Inspired by Muscle Training. *Science.* **2019**, 363 (6426), 504–508.
- (19) Yang, J.; Bai, R.; Suo, Z. Topological Adhesion of Wet Materials. *Adv. Mater.* **2018**, 30 (25), 1–7.
- (20) Huebsch, N.; Kearney, C. J.; Zhao, X.; Kim, J.; Cezar, C. A.; Suo, Z.; Mooney, D. J. Ultrasound-Triggered Disruption and Self-Healing of Reversibly Cross-Linked Hydrogels for Drug Delivery and Enhanced Chemotherapy. *Proc. Natl. Acad. Sci. U. S. A.* **2014**, 111 (27), 9762–9767.
- (21) Zhao, X.; Kim, J.; Cezar, C. A.; Huebsch, N.; Lee, K.; Bouhadir, K.; Mooney, D. J. Active Scaffolds for On-Demand Drug and Cell Delivery. *Proc. Natl. Acad. Sci. U. S. A.* **2011**, 108 (1), 67–72.
- (22) Wang, E.; Desai, M. S.; Lee, S. W. Light-Controlled Graphene-Elastin Composite Hydrogel

- Actuators. Nano Lett. 2013, 13 (6), 2826–2830.
- (23) Illeperuma, W. R. K. K.; Sun, J.-Y. Y.; Suo, Z.; Vlassak, J. J. Force and Stroke of a Hydrogel Actuator. *Soft Matter* **2013**, 9 (35), 8504–8511.
- (24) Baumgartner, R.; Kogler, A.; Stadlbauer, J. M.; Foo, C. C.; Kaltseis, R.; Baumgartner, M.; Mao, G.; Keplinger, C.; Koh, S. J. A.; Arnold, N.; Suo, Z.; Kaltenbrunner, M.; Bauer, S. A Lesson from Plants: High-Speed Soft Robotic Actuators. *Adv. Sci.* **2020**, 7 (5).
- (25) Ionov, L. Hydrogel-Based Actuators: Possibilities and Limitations. *Mater. Today* **2014**, 17 (10), 494–503.
- (26) Kim, Y.; Parada, G. A.; Liu, S.; Zhao, X. Ferromagnetic Soft Continuum Robots. *Sci. Robot.* **2019**, 4 (33), eaax7329.
- (27) Blacklow, S. O.; Li, J.; Freedman, B. R.; Zeidi, M.; Chen, C.; Mooney, D. J. Bioinspired Mechanically Active Adhesive Dressings to Accelerate Wound Closure. *Sci. Adv.* **2019**, 5 (7).
- (28) Sun, J. Y.; Zhao, X.; Illeperuma, W. R.; Chaudhuri, O.; Oh, K. H.; Mooney, D. J.; Vlassak, J. J.; Suo, Z. Highly Stretchable and Tough Hydrogels. *Nature* **2012**, 489 (7414), 133–136.
- (29) Li, J.; Celiz, A. D.; Yang, J.; Yang, Q.; Wamala, I.; Whyte, W.; Seo, B. R.; Vasilyev, N. V.; Vlassak, J. J.; Suo, Z.; Mooney, D. J. Tough Adhesives for Diverse Wet Surfaces. *Science*. **2017**, 357 (6349), 378–381.
- (30) Schild, H. G. Poly(N-Isopropylacrylamide): Experiment, Theory and Application. *Prog. Polym. Sci.* **1992**, 17 (2), 163–249.
- (31) Hong, W.; Zhao, X.; Zhou, J.; Suo, Z. A Theory of Coupled Diffusion and Large Deformation in Polymeric Gels. *J. Mech. Phys. Solids.* **2008**, 56 (5), 1779–1793.
- (32) Cai, S.; Suo, Z. Mechanics and Chemical Thermodynamics of Phase Transition in Temperature-Sensitive Hydrogels. *J. Mech. Phys. Solids.* **2011**, 59 (11), 2259–2278.
- (33) Hong, W.; Liu, Z.; Suo, Z. Inhomogeneous Swelling of a Gel in Equilibrium with a Solvent and Mechanical Load. *Int. J. Solids Struct.* **2009**, 46 (17), 3282–3289.
- (34) Flory, P. J. *Principles of Polymer Chemistry*; Cornell University Press: Ithaca, N.Y., **1953**.
- (35) Flory, P. J. Themodynamics of High Polymer Solutions. J. Chem. Phys. **1942**, 10 (1), 51–61.
- (36) Huggins, M. L. Solutions of Long Chain Compounds. J. Chem. Phys. 1941, 9, 440.
- (37) Huggins, M. L. A Revised Theory of High Polymer Solutions. J. Am. Chem. Soc. 1964, 86 (17), 3535–3540.
- (38) Li, Z.; Liu, Z.; Ng, T. Y.; Sharma, P. The Effect of Water Content on the Elastic Modulus and Fracture Energy of Hydrogel. *Extrem. Mech. Lett.* **2020**, 35.
- (39) Li, J.; Hu, Y.; Vlassak, J. J.; Suo, Z. Experimental Determination of Equations of State for Ideal Elastomeric Gels. *Soft Matter* **2012**, 8 (31).
- (40) RIVILIN. Rupture of Rubber. 1. Characteristic Energy for Tearing. *J. Polym. Sci.* **1953**, 10 (3).
- (41) Kendall, K. Thin-Film Peeling the Elastic Term. J. Phys. D: Appl. Phys. 1975, 8.
- (42) Qi, Y.; Caillard, J.; Long, R. Fracture Toughness of Soft Materials with Rate-Independent Hysteresis. *J. Mech. Phys. Solids* **2018**, 118, 341–364.
- (43) Zhang, T.; Lin, S.; Yuk, H.; Zhao, X. Predicting Fracture Energies and Crack-Tip Fields of Soft Tough Materials. *Extrem. Mech. Lett.* **2015**, 4.
- (44) Yang, C.; Yin, T.; Suo, Z. Polyacrylamide Hydrogels. I. Network Imperfection. *J. Mech. Phys. Solids* **2019**, 131, 43–55.
- (45) Cai, S.; Suo, Z. Equations of State for Ideal Elastomeric Gels. *Epl* **2012**, 97 (3).

- (46) Hoshino, K. I.; Nakajima, T.; Matsuda, T.; Sakai, T.; Gong, J. P. Network Elasticity of a Model Hydrogel as a Function of Swelling Ratio: From Shrinking to Extreme Swelling States. *Soft Matter* **2018**, 14 (47), 9693–9701.
- (47) Sakai, T.; Kurakazu, M.; Akagi, Y.; Shibayama, M.; Chung, U. Il. Effect of Swelling and Deswelling on the Elasticity of Polymer Networks in the Dilute to Semi-Dilute Region. *Soft Matter* **2012**, 8 (9), 2730–2736.
- (48) Tang, J.; Li, J.; Vlassak, J. J.; Suo, Z. Fatigue Fracture of Hydrogels. *Extrem. Mech. Lett.* **2017**, 10, 24–31.
- (49) Ni, X.; Yang, Z.; Li, J. Scaling Behavior of Fracture Properties of Tough Adhesive Hydrogels. *ACS Macro Lett.* **2021**, 10(2), 180-185.
- (50) Suo, Z.; Hutchinson, J. W. Interface Crack between Two Elastic Layers. *Int. J. Fract.* **1990**, 43, 1–18.
- (51) Hui, C. Y.; Ruina, A.; Long, R.; Jagota, A. Cohesive Zone Models and Fracture. *J. Adhes.* **2011**, 87 (1), 1–52.
- (52) Tvergaard, V.; Hutchinson, J. W. On the Toughness of Ductile Adhesive Joints. *J. Mech. Phys. Solids* **1996**, 44 (5), 789–800.
- (53) Wei, Y.; Hutchinson, J. W. Interface Strength, Work of Adhesion and Plasticity in the Peel Test. *Int. J. Fract.* **1998**, 93 (1–4), 315–333.
- (54) Yuk, H.; Zhang, T.; Lin, S.; Parada, G. A.; Zhao, X. Tough Bonding of Hydrogels to Diverse Non-Porous Surfaces. *Nat Mater* **2016**, 15 (2), 190–196.
- (55) Zhang, T.; Yuk, H.; Lin, S.; Parada, G. A.; Zhao, X. Tough and Tunable Adhesion of Hydrogels: Experiments and Models. *Acta Mech. Sin.* **2017**, 33 (3), 543–554.
- (56) Long, R.; Hui, C. Y. Fracture Toughness of Hydrogels: Measurement and Interpretation. *Soft Matter* **2016**, 12 (39), 8069–8086.
- (57) Newby, B. -m. Z.; Chaudhury, M. K.; Brown, H. R. Macroscopic Evidence of the Effect of Interfacial Slippage on Adhesion. *Science*. **1995**, 269 (5229), 1407–1409.
- (58) Marcombe, R.; Cai, S.; Hong, W.; Zhao, X.; Lapusta, Y.; Suo, Z. A Theory of Constrained Swelling of a PH-Sensitive Hydrogel. *Soft Matter* **2010**, 6 (4).

# **SUPPORTING INFORMATION**

## Stimulation modulates adhesion and mechanics of hydrogel adhesives

Zhen Yang a‡, Xingwei Yang b‡, Rong Long b\*, Jianyu Li ac\*

<sup>a</sup>Department of Mechanical Engineering, McGill University, Montreal, QC H3A 0C3, Canada <sup>b</sup>Department of Mechanical Engineering, University of Colorado Boulder, Boulder, CO 80309, USA.

<sup>c</sup>Department of Biomedical Engineering, McGill University, Montreal, QC H3A 0C3, Canada

<sup>‡</sup>These authors contributed equally to this work

This file includes:

Materials

Table S1

Additional information on experiments

Figure S1

Figure S2

Figure S3

Figure S4

Figure S5

Additional information on finite element modeling

Figure S6

Figure S7

Figure S8

Figure S9

Figure S10

Additional information on analytical model

Figure S11

Figure S12

Schematic of stimuli-responsive hydrogel adhesive - tissue adhesion

Figure S13

<sup>\*</sup> Corresponding authors

#### **Materials**

**Materials.** Chemicals used in this work were purchased without further purification. Poly(N-isopropylacrylamide) (NIPAm, monomer) was purchased from TCI (Portland, USA); N,N'-methylenebis (acrylamide) (MBAA, covalent crosslinker), N,N,N',N'tetramethylethylenediamine (TEMED, accelerator), ammonium persulfate (APS, initiator), calcium sulfate (ionic crosslinker), N-hydroxysulfosuccinimide (NHS), and 1-ethyl-3-(3dimethylaminopropyl) carbodiimide (EDC) were purchased from Sigma Aldrich (St. Louis, Missouri, USA). Alginate (I-1G) was purchased from KIMICA Corporation (Tokyo, Japan). Chitosan (deacetylation degree 95%, medium to high molecular weight) was purchased from Xi'an Lyphar Biotech (Shanxi, China). Glass and acrylic sheets were purchased from McMaster-Carr to make reaction molds. Collagen casing was purchased from a local grocery store and then stored in the fridge at 4°C before use.

**Synthesis of stimuli-responsive hydrogel adhesive.** Following previously reported protocols<sup>1,2</sup>, the stimuli-responsive adhesive is made of two layers: a dissipative matrix made of PNIPAm/alginate hydrogel and a topohesive surface (chitosan, EDC and NHS) to form a bridging network with tissues. To synthesize the hydrogel, 6.3 g of NIPAm monomers and 1 g of sodium alginate were first dissolved in 50 mL of deionized water. Then, 10 ml of the NIPAm-alginate solution was mixed with 22.54 μL of MBAA aqueous solution (0.28 mM) and 5.8 μL of TEMED (3.7 mM) within a syringe. Meanwhile, 234.7 μL of APS solution (6.5 mM) and 179.72 μL calcium sulfate slurries (CaSO<sub>4</sub>, 0.15M) were mixed in another syringe. The two syringes were connected with a Luer Lock connector and syringe-mixed quickly to form a homogeneous solution. The mixture was immediately injected into a mold with 80×15×1.5 mm³ in size, covered with a glass plate and subsequently kept at 4 °C for 24 hours to complete the reaction. The same procedure was followed for synthesizing the PNIPAm/alginate single-network (SC) hydrogel, except that the calcium sulfate slurries were replaced by deionized water of the same volume.

To prepare the topohesive surface, 1 g of chitosan powder was firstly dissolved in 50 mL deionized water with 400  $\mu$ L of acetic acid for a final pH of 4.5. The mixture was stirred overnight to form a homogenous solution and then kept at 4 °C before use. Then, varying concentrations (0, 2 and 6% w/v) of coupling reagents (EDC and NHS at equal weights) were added into 1 mL of the 2% w/v chitosan solution to tune the level (Table S1).

Fabrication of the model tissue. We fabricated a model tissue substrate with a collagen casing and an acrylic sheet. The dry collagen casing was soaked in deionized water for 30 minutes and subsequently glued onto the acrylic sheet (Figure S1). The model tissue provides abundant amino and carboxyl groups from collagen casing for covalent bonding with the adhesive. It is considered as a rigid substrate due to the high elastic modulus of the acrylic (on the order of 1 GPa). Also, the model tissue is flat and smooth. The hydrogel adhesives were attached onto the model tissues with topohesives of varying chemical reagent inputs, while other conditions, for example, the applied compression and the reaction time, were kept the same. An initial crack of 15 mm was introduced near the one end of the sample, and the length of the overlapping joint was 65 mm for adhesion energy measurements. After the placement of the adhesive, the samples were

clamped between two acrylic sheets for compression and then stored in a seal bag at 4  $^{\circ}\mathrm{C}$  for 24 hours.

Table S1: Composition of coupling reagents added onto stimuli-responsive adhesives for tissue adhesion

| Sample | Amounts of reagents (EDC+NSH) (mg) | 2% w/v chitosan +varying concentration coupling reagents |
|--------|------------------------------------|--|
| 1      | 60                                 | 6% w/v   |
| 2      | 20                                 | 2% w/v   |
| 3      | 0                                  | $0\% \mathrm{w/v}$                                       |

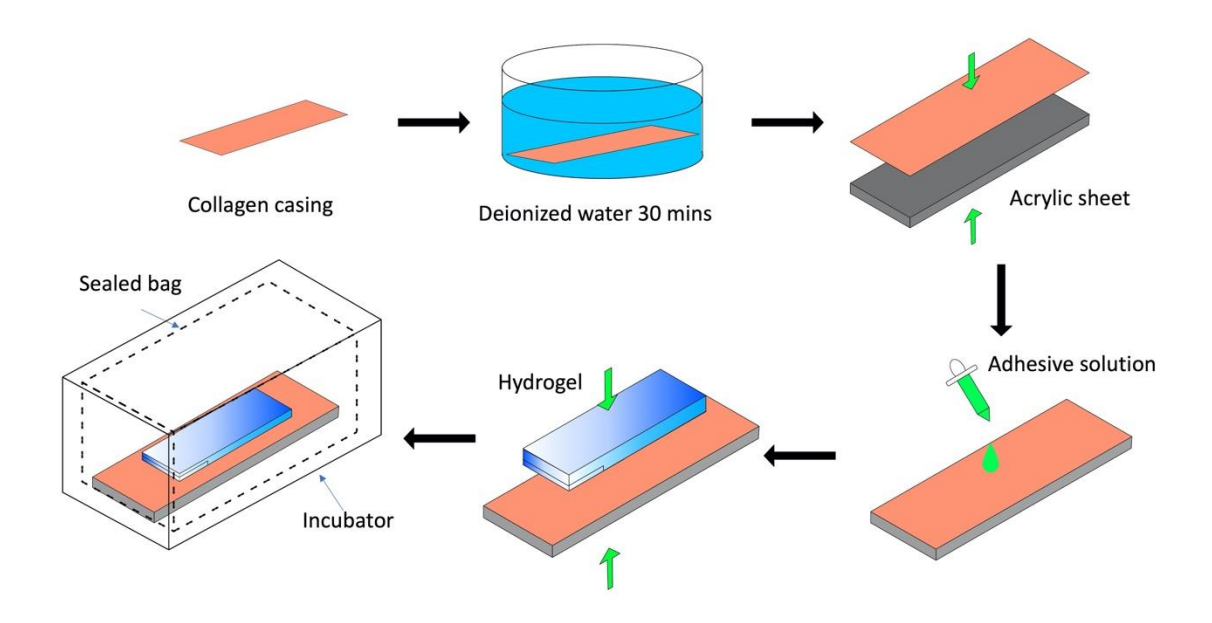


Figure S1 Fabrication of the model tissue and the application of the stimuli-responsive adhesive. The stimulation is realized by placing the specimen in an incubator of 37 °C.

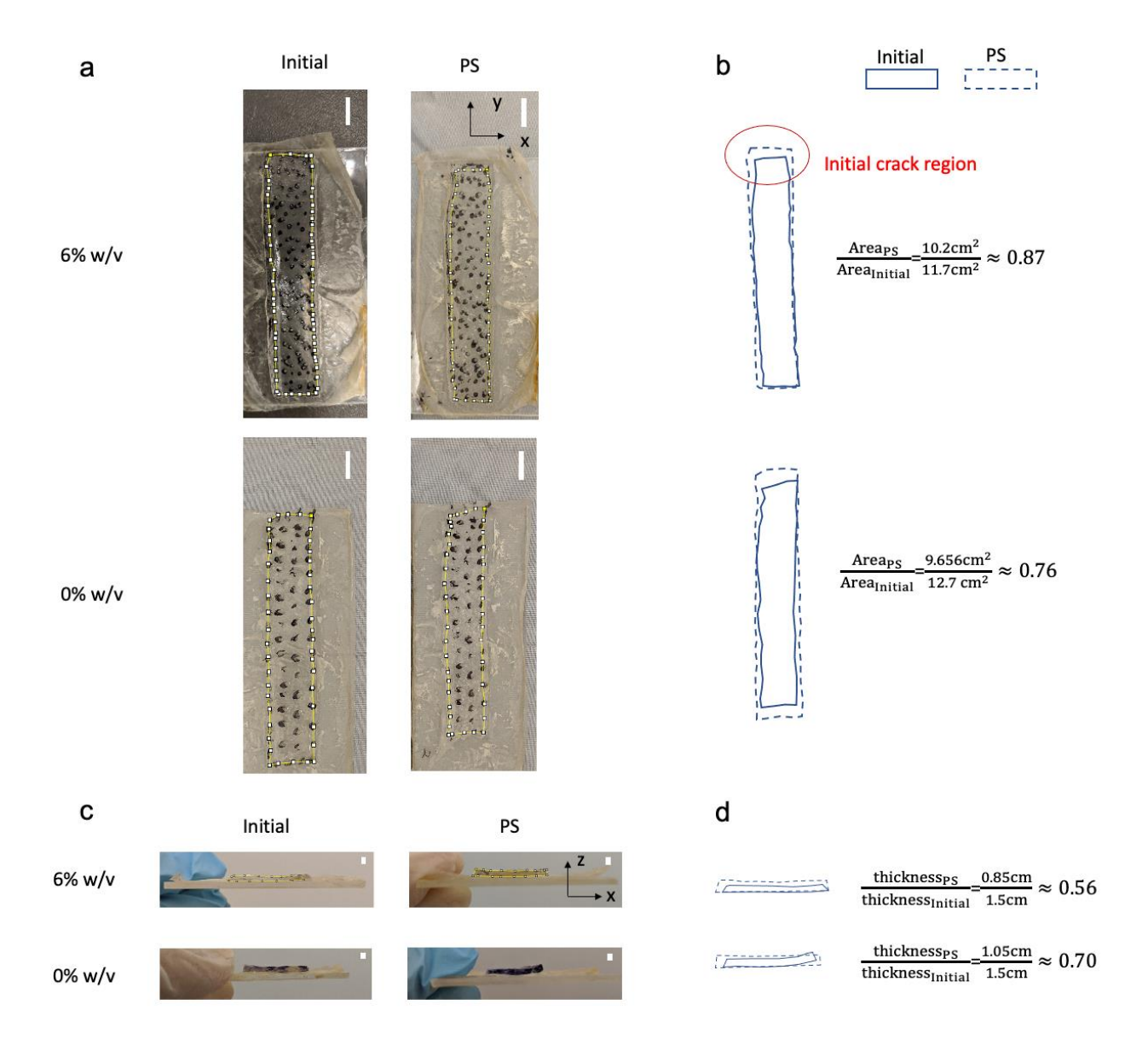


Figure S2 Images and contours of the stimuli-responsive adhesive adhered onto the model tissue substrate before and after stimulation. (a) Images of the stimuli-responsive adhesive before and after stimulation and the contours (b) overlaid in the x-y plane. Scale bar, 1 cm. The ratio of the contour areas is calculated. The strong adhesion formed with 6% w/v coupling reagents results in in-plane contraction (area ratio ~0.87) limited to the initial crack region. Without any coupling reagent, the adhesion is weaker, enabling substantial in-plane contraction (area ratio ~0.76) at all edges of the specimen. (c) Images and (d) cross-sectional profiles of the stimuli-responsive adhesive before and after the stimulation in the x-z plane. Scale bar, 1.65 mm. The profiles shown in (d) is magnified for better illustration. The thickness reduction with 6% w/v reagent is slightly larger than that with 0% w/v reagent. Notably, one end of the adhesive with 0% reagent tilts up upon stimulation, indicative of delamination.

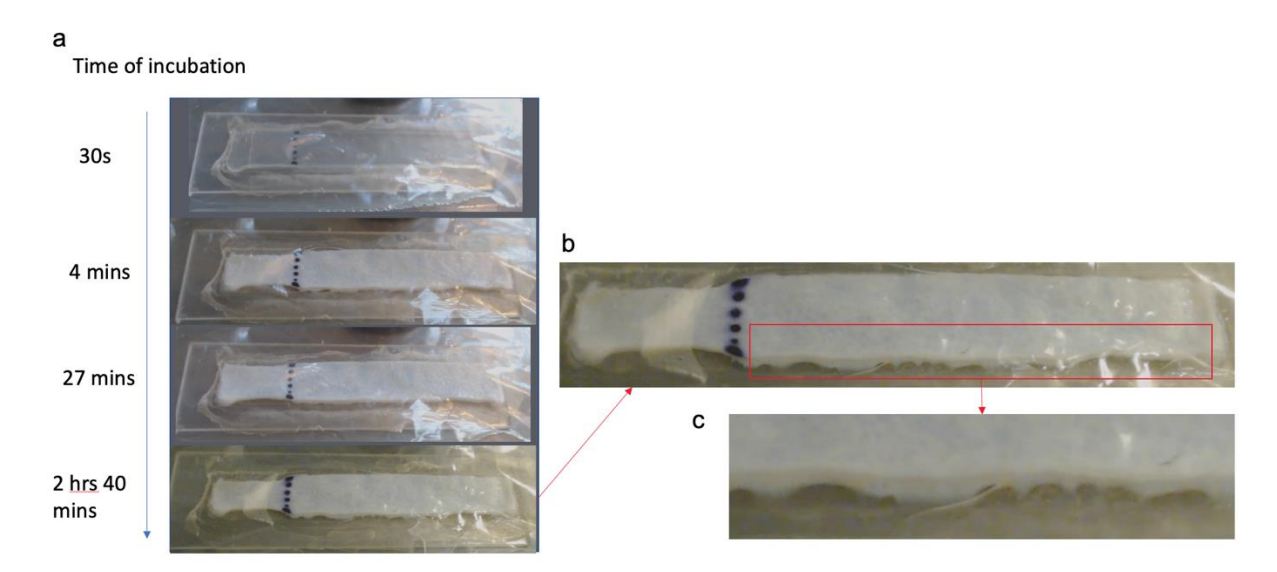


Figure S3 Time series images of the stimuli-responsive adhesive with 2%w/v reagents. (a) plots deformation change with incubation time. (b) Enlarged view of the adhesive hydrogel at 2hrs 40 mins in (a). (c) Enlarged view of the highlighted region in (b), showing localized debonding near the edge of the interface.

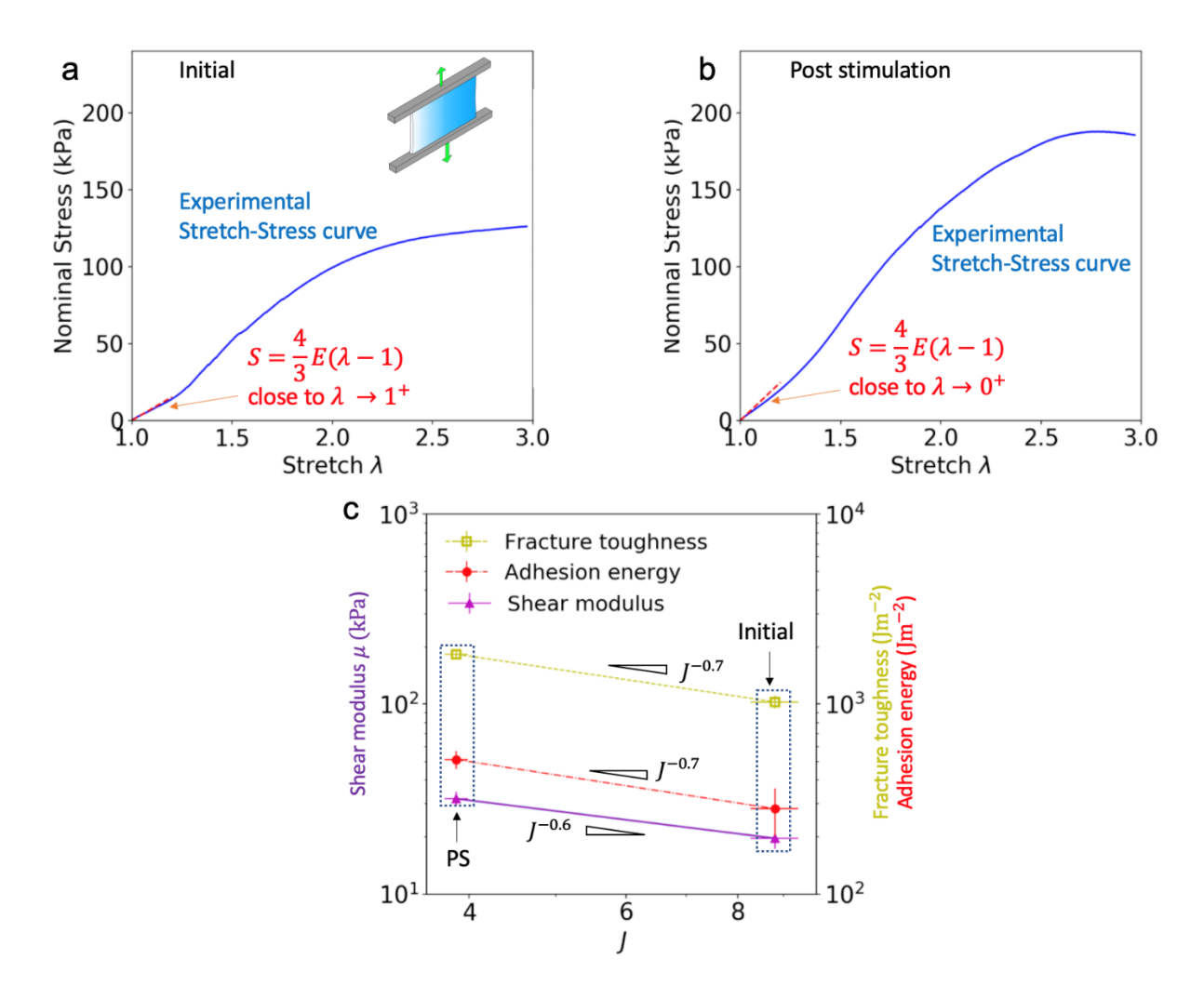
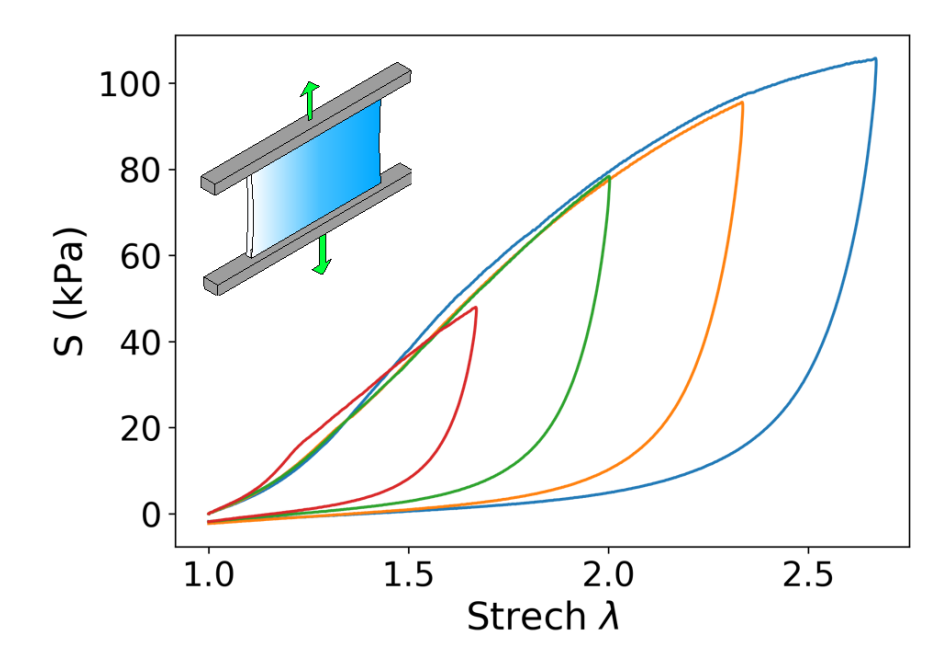


Figure S4 Stress-stretch curves of the stimuli-responsive adhesive before and after stimulation in pure shear tests. Representative nominal stress-stretch curves for the initial (a) and the post stimulation (b) states. The elastic modulus is measured by assessing the slope of the initial portion of the curve,  $\partial S/\partial(\lambda-1)=4E/3$ . (c) Adhesion energy, bulk fracture energy and shear modulus plotted as functions of swelling ratio J. The adhesion energy corresponding to the case with topohesives containing 6% w/v reagents. Sample size n=3.



**Figure S5** Nominal stress-stretch curves for the PNIPAm/alginate DC hydrogels in a pure shear specimen (inset) loaded up to different stretches. The loading-unloading curves form hysteresis loops, indicative of significant energy dissipation.

## ADDITIONAL INFORMATION ON FINITE ELEMENT MODELING

Finite element (FE) simulations were performed using the commercial software ABAQUS (version 2020, Simulia, Providence, RI, USA). Below described are two types of simulations performed in this work, i.e., free swelling and interface debonding.

Free swelling. A cubic block,  $8 \times 8 \times 8 \text{mm}^3$  in size, was used to represent the DC hydrogel in the FE model and was meshed using the 3D continuum element C3D8HT (512 elements in total). The hydrogel was subjected to a temperature change from 294K to 320K throughout the simulation. The simulations were performed using the coupled temperature-displacement analysis. Figure S6 shows the volume change of the hydrogel block in the FE model, when the temperature is elevated. The FE results is compared with the analytical estimation of the equilibrium swelling ratio J curve, i.e., the fitting function H(J, T) for the shear modulus of the hydrogel  $\mu = 19$  kPa. The two results show a good agreement. Moreover, the experimental results for the swelling test of the as-prepared DC hydrogel is also plotted in Figure S6 for comparison, showing a qualitative agreement with both the FE and the analytical results. The quantitative difference is due to the fact that the as-prepared DC hydrogel is not in swelling equilibrium under the room temperature, nor under 320 K due to the limited stimulation time.

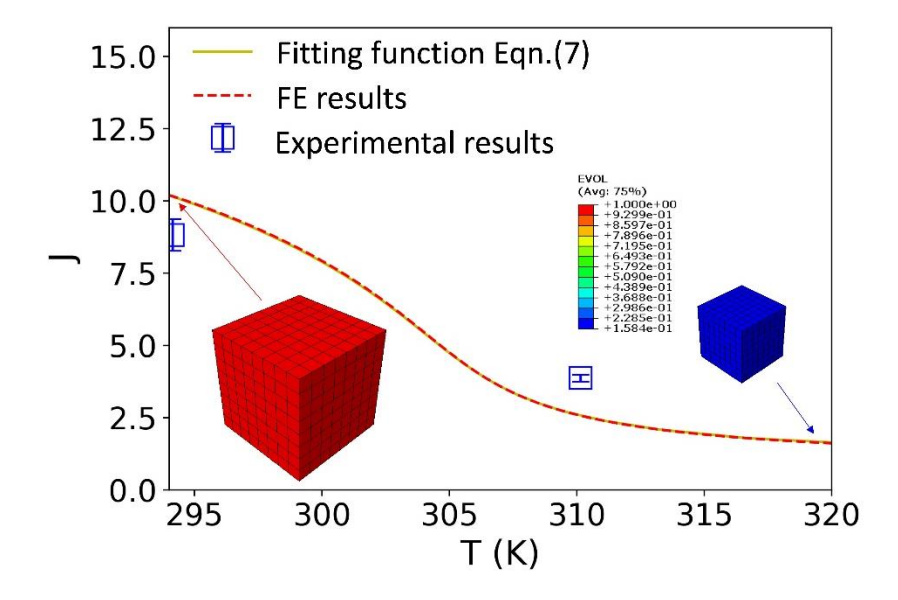


**Figure S6 Equilibrium swelling ratio** *J*: analytical estimate (solid line), FE results (dashed line) and experimental data (symbols). The insets illustrate the volumetric deformation of a hydrogel cube subjected to the temperature increase. The color contour shows the swelling ratio defined as EVOL, the ratio of the current volume versus the initial volume.

**Interface debonding**. A two-dimensional plane strain model was developed to study the interface debonding between the hydrogel adhesive and the model tissue. The model consists of a hydrogel adhesive on a substrate representing the model tissue [Figure S7]. The substrate was

modelled as a rigid body with the bottom surface fixed in all degrees of freedom. The hydrogel adhesive was modelled using the Flory-Rhener free energy function [Eqn. (1) – (4)] via the UHYPER user subroutine. The interface between the hydrogel adhesive and the model tissue was modelled using a cohesive zone model, which was defined by prescribing a relation between the mechanical traction and the relative separation between the two contacting surfaces.<sup>3</sup> Here we adopted a simple bilinear traction-separation law for the cohesive zone model, as illustrated in Figure S7. The cohesive zone model features a few parameters:  $\delta_f$  and  $\sigma_{max}$  are the maximum separation and strength, respectively, while K is the initial stiffness and  $G_c = \sigma_{max} \delta_f/2$  is the area underneath the traction-separation curve, representing the adhesion energy between the interface. Complete interface failure occurs when  $\delta_f$  is reached and the traction reduces to 0. In this work, we used  $\delta_f = 0.5$  mm and  $K = 10^{11}$  N/ $m^3$ . The schematic in Figure S7 only shows the traction-separation law along one direction. However, in simulations the interface is subjected to tractions both in its normal and tangential directions. To account for tractions in these two directions, we used the following quadratic stress criterion for the damage initiation:

$$\left(\frac{\sigma_{\rm n}}{\sigma_{\rm n,max}}\right)^2 + \left(\frac{\sigma_{\rm t}}{\sigma_{\rm t,max}}\right)^2 = 1, \tag{S1}$$

with  $\sigma_n$  and  $\sigma_t$  representing tractions normal and tangential to the interface, respectively. As mentioned in the main text, two types of cohesive zone models were used: i) mode-independent, and ii) Mode-I dominant. In the former model, we set  $\sigma_{n,\text{max}} = \sigma_{t,\text{max}}$  and  $G_c$  depends on both the normal and tangential directions in an isotopic manner. In the latter model, we set  $\sigma_{n,\text{max}} =$  $20\sigma_{t,\text{max}}$  such that the adhesion energy  $G_c$  is dominated by traction along the normal direction. In the simulations, the hydrogel adhesive and substrate were initially at 294K. They were subjected to a temperature increase until the crack started to propagate on the interface, after which the temperature was held until most of the interface (i.e., >90% in area) delaminates. Different adhesion energies  $G_c$  were prescribed to determine the temperature at the onset of interface crack propagation. Examples showing the deformed configurations of the mode-independent and Mode-I dominant cases are shown in Figure S8 and Figure S9, respectively. In the mode-independent case, we observed that the deformed crack surface deflected forward and exhibited a fingertip-like shape [Figure S8 (a) and (b)), leading to the excessive distortion in the elements near the crack tip and causing convergence issue. As a result, for the mode-independent case, the 6-node modified displacement and temperature element CPE6MHT was used [Figure S8(c)] to suppress mesh distortion. The size of the element was set to be uniformly 0.25 mm, which was half of  $\delta_f$  and capable of capturing the interfacial behavior of the system. In the Mode-I dominant case, the absence of the fingertip-like shape near the crack tip enables us to use a more refined mesh to capture the large deformation of the hydrogel near the interface. The 4-node bilinear displacement and temperature element CPE4HT with a transition mesh [Figure S9(c)] was adopted for the hydrogel with the smallest element size being ~0.03 mm. In addition to the pre-existing crack at the left side of the hydrogel, a new crack can initiate and propagate from the right edge of the hydrogel [Figure S8(a) and S9(a)]. The critical temperature at the onset of crack propagation were extracted from FE simulations based on the damage parameter of the cohesive zone. Once the damage parameter of the first few cohesive elements near the crack tip reaches 1, the crack, either the pre-existing one or the new one initiated at the right edge, can propagate steadily. Figure S10 shows the energy release rate G versus temperature for the two cases with mode-independent and Mode-I dominant cohesive zone models. The energy releaser rate for the pre-existing crack (left edge) and the new crack initiated (right edge) are close to each other, especially for relative high temperature (e.g., T > 305 K). For consistency, we adopted the results for the pre-existing crack in Figure 5 of the main text.

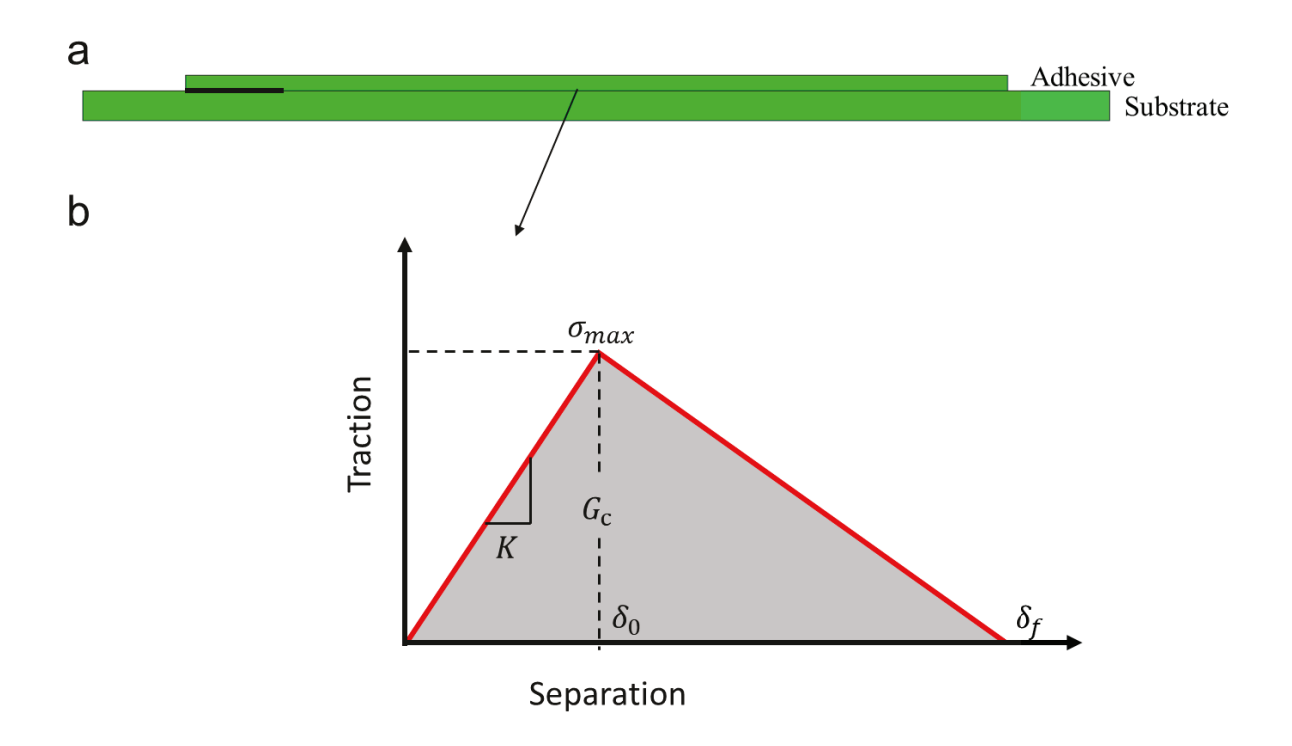


**Figure S7 FE model geometry and cohesive zone.** (a) The FE model consists of a hydrogel adhesive bonded to the top of a rigid substrate. (b) Adhesion on the interface between the hydrogel adhesive and the substrate is simulated using a cohesive zone model with bilinear traction-separation law.

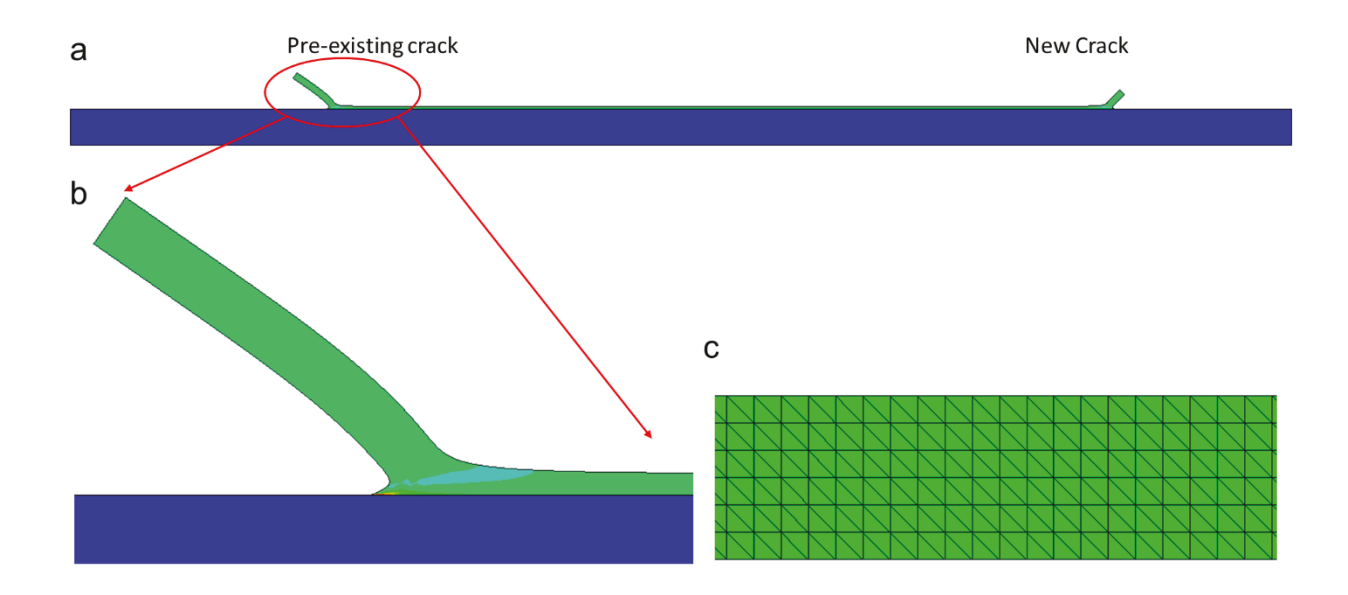


**Figure S8 FE model with mode independent cohesive zone.** (a) A representative deformation profile of the hydrogel adhesive. (b) Zoomed-in view of the crack tip. (c) Mesh used in the hydrogel adhesive.

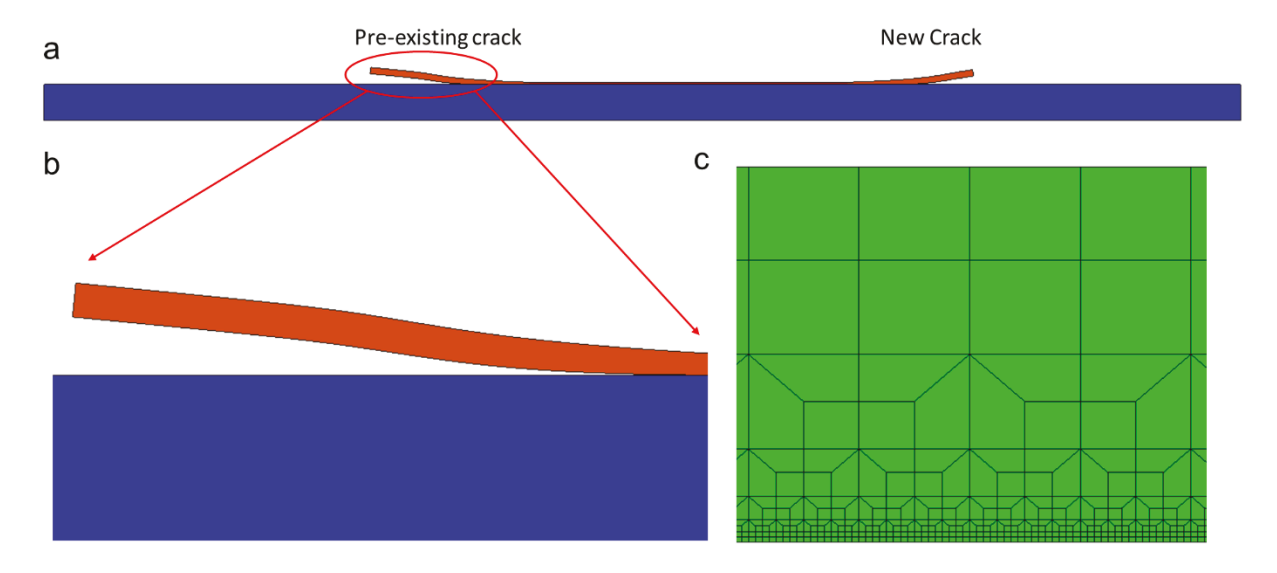


**Figure S9 FE model with the Mode-I dominant cohesive zone.** (a) A representative deformation profile of the hydrogel adhesive. (b) Zoomed-in view of the crack tip. (c) Mesh used in the hydrogel adhesive.

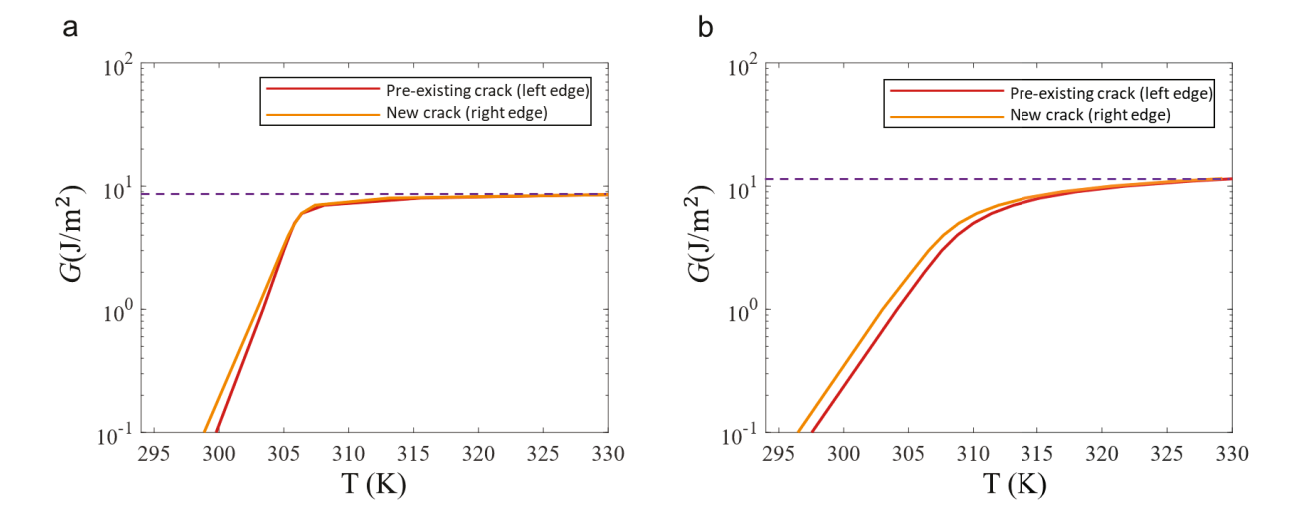


Figure S10 Energy release rate under temperature increase. (a) The energy release rate G for both the pre-existing crack (left edge) and the new crack (right edge) using the mode independent cohesive zone. (b) The energy release rate G for both the pre-existing crack (left edge) and the new crack (right edge) using the Mode-I dominant cracks. The dashed lines in (a-b) represent the maximum values of G found in the simulation.

## ADDITIONAL INFORMATION ON ANALYTICAL MODELING

**Interface crack between two elastic layers.** In Suo and Hutchinson<sup>4</sup>, the strain energy release rate *G* is given by:

$$G = \frac{1}{8\mu} \left[ \frac{P^2}{Ah_1} + \frac{M^2}{Ih_1^3} + 2\frac{PM}{\sqrt{AI}h_1^2} \sin \gamma \right]$$
 (S2)

with the geometrical factors given by:

$$\frac{1}{A} = 1 + \Sigma \left( 4\eta + 6\eta^2 + 3\eta^3 \right)$$

$$\Sigma \approx 0, \text{ due to the rigid substrate}$$

$$\frac{1}{I} = 12(1 + \eta^3)$$

$$\frac{\sin \gamma}{\sqrt{AI}} = 6\eta^2 \left( 1 + \eta \right)$$
(S3)

where  $\eta = \frac{h_1}{h_2}$  ( $h_1$  and  $h_2$  are the thickness of the hydrogel adhesive and the model tissue, respectively). We set  $\eta = 1$  based on the dimensions of the specimen in the experiment. In our problem, the actual loadings and moments applied to the specimen are shown in Figure S11:

$$P_{1} = -P_{3} = P$$
 $M_{1} = M_{2} = 0$ 
 $M_{3} = P_{r} \left( h_{2} - \delta + \frac{h_{1}}{2} \right)$ 
(S4)

The equivalent loads and moments are shown in Figure 5(a):

$$P = P_r = S_r h_1,$$

$$M = 0$$
(S5)

Substituting Eqn.(S5) into (S2) yields Eqn.(10).

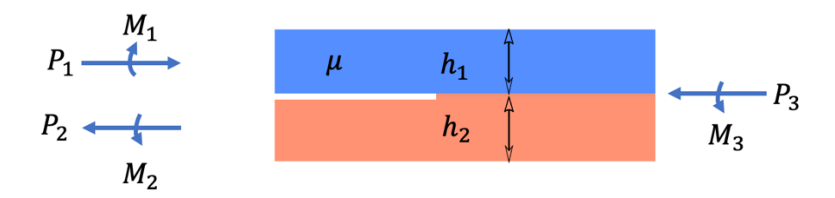


**Figure S11** schematic of the interfacial crack embedded in a bi-material specimen subjected to the general loadings.

# Estimation of residual stress $S_r$ in the adhesive hydrogel under phase transition.

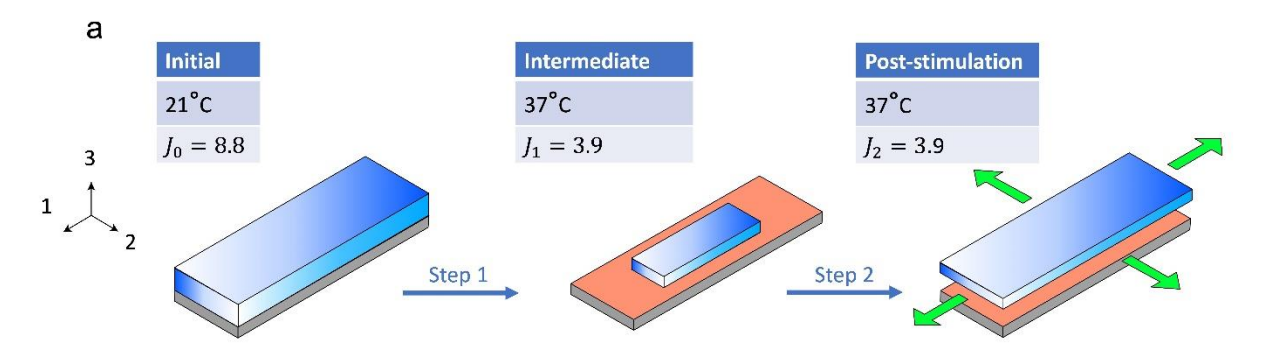


**Figure S12** schematic illustrating the stretch-and-fit procedure. Axes 1, 2, are parallel to the interface while axis 3 is normal to the interface.

To estimate residual stress, we consider an imaginary two-step process [Figure 4(c)]. The hydrogel adhesive is initially under the room temperature with the swelling ratio  $J_0 = 8.8$ . In the first step, its temperature increases to 310 K and it shrinks freely to the intermediate state with the swelling ratio  $J_1 = 3.9$ . In the second step, the shrunken hydrogel adhesive is biaxially stretched by  $\lambda$  in directions 1 and 2 with respect to the dry polymer state and fitted onto the tissue substrate such that  $\lambda = (J_0/J_1)^{1/3} = 1.31$ . The deformation gradient reads

$$\mathbf{F} = \lambda \mathbf{e}_1 \otimes \mathbf{e}_1 + \lambda \mathbf{e}_2 \otimes \mathbf{e}_2 + \frac{1}{\lambda^2} \mathbf{e}_3 \otimes \mathbf{e}_3$$
 (S6)

If assuming the hydrogel adhesive can be described by a Neo-Hookean material, the true stress is given by:

$$\mathbf{\sigma} = \mu_{PS} \left( \mathbf{F} \mathbf{F}^{T} - \mathbf{I} \right) + p \mathbf{I} = \left[ \mu_{PS} \left( \lambda^{2} - 1 \right) + p \right] \mathbf{e}_{1} \otimes \mathbf{e}_{1} + \left[ \mu_{PS} \left( \lambda^{2} - 1 \right) + p \right] \mathbf{e}_{2} \otimes \mathbf{e}_{2} + \left[ \mu_{PS} \left( \frac{1}{\lambda^{4}} - 1 \right) + p \right] \mathbf{e}_{3} \otimes \mathbf{e}_{3}$$
(S7)

The hydrostatic pressure p can be calculated using the fact that the hydrogel is stress free in the out-of-plane direction:  $\mu_{PS}\left(\frac{1}{\lambda^4}-1\right)+p=0$ . Taken together, the true stress component in the biaxial directions (direction 1 and 2 in Figure S12) is given by:

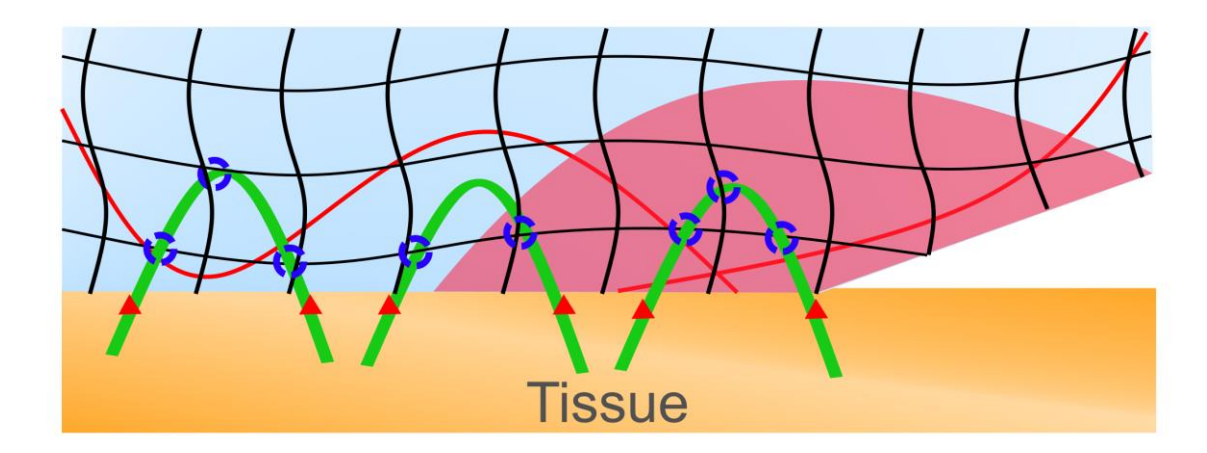
$$\sigma_r = \mu_{\rm PS} \left( \lambda^2 - \frac{1}{\lambda^4} \right) \tag{S8}$$

As well, under biaxial stretch the nominal stress is associated with the true stress by  $S_r\lambda = \sigma_r$ :

$$S_r = \mu_{PS} \left( \lambda - \frac{1}{\lambda^5} \right) \tag{S9}$$

By substituting values of  $\mu_{PS}$  and  $\lambda$  into Eqn. (S9),  $S_r$  is estimated to be 33 kPa.

# SCHEMATIC OF STIMULI-RESPONSIVE HYDROGEL ADHESIVE-TISSUE ADHESION



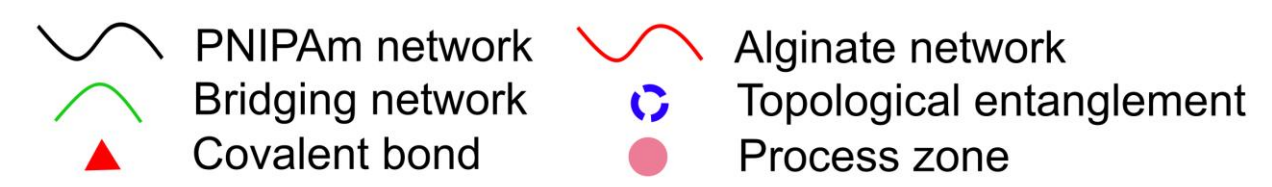


Figure S13 Schematic showing the adhesion between the adhesive hydrogel and the tissue surface. The adhesion is established by the bridging network (chitosan) with its one end in topological entanglement with the hydrogel network, and the other end covalently bonded on the tissue surface. Upon an interfacial delamination, a process zone formed near the crack tip, in which significant amount of alginate network breaks, leading to energy dissipation.

## References

- (1) Blacklow, S. O.; Li, J.; Freedman, B. R.; Zeidi, M.; Chen, C.; Mooney, D. J. Bioinspired Mechanically Active Adhesive Dressings to Accelerate Wound Closure. *Sci. Adv.* **2019**, *5* (7).
- (2) Li, J.; Celiz, A. D.; Yang, J.; Yang, Q.; Wamala, I.; Whyte, W.; Seo, B. R.; Vasilyev, N. V.; Vlassak, J. J.; Suo, Z.; Mooney, D. J. Tough Adhesives for Diverse Wet Surfaces. *Science* **2017**, *357* (6349), 378–381.
- (3) Hui, C. Y.; Ruina, A.; Long, R.; Jagota, A. Cohesive Zone Models and Fracture. *J. Adhes.* **2011**, 87 (1), 1–52.
- (4) Suo, Z.; Hutchinson, J. W. Interface Crack between Two Elastic Layers. *Int. J. Fract.* **1990**, *43*, 1–18.